NF-κB-Inducing Kinase Rewires Metabolic Homeostasis and Promotes Diet-Induced Obesity

Authors: Kathryn M. Pflug[1, 2], Dong W. Lee[1], Raquel Sitcheran[1, 2, *]

Affiliations:

[1] Department of Molecular & Cellular Medicine, Texas A&M University Health Science Center, College Station TX 77845, USA

[2] Interdisciplinary Graduate Program in Genetics, Texas A&M University, College Station TX 77845, USA

* Correspondence: sitcheran@tamu.edu

Keywords

NF-κB-inducing kinase, NIK, Map3k14, NF-κB, Metabolism, Glycolysis, Extracellular Acidification Rate (ECAR), Oxidative Phosphorylation (OXPHOS), Oxygen Consumption Rate (OCR), Spare Respiratory Capacity, Proton Leak, Adipogenesis, PPARγ, C/EBPα, High-Fat Diet, Adipose Expansion, Insulin Sensitivity, Metabolic Syndrome, Obesity

Abstract

Obesity is a predominant risk factor for metabolic syndrome, which refers to a cluster of disorders that include diabetes, cardiovascular disease and fatty liver disease. Obesity and overnutrition are associated with aberrant immune and inflammatory responses resulting in increased local fat deposition, insulin resistance and systemic metabolic dysregulation. Here we show NF-κB-inducing kinase (NIK), a critical regulator of immunity and inflammation has local and systemic effects on metabolic processes. We demonstrate that NIK has NF-κB-independent and -dependent roles on adipose development and function. Independently of noncanonical NF-κB, NIK deficiency regulates mitochondrial spare respiratory capacity (SRC) and proton leak but establishes higher basal oxygen consumption and glycolytic capacity in preadipocytes and *ex vivo* adipose tissue. In addition, we demonstrate NIK promotes adipogenesis through its role in activation of the noncanonical NF-κB pathway. Strikingly, when challenged with a high fat diet, NIK deficient mice are protected against diet-induced obesity and insulin insensitivity. Overall, mice lacking NIK exhibit decreased overall fat mass and increased energy expenditure. Our results establish that, through its influences on adipose development, metabolic homeostasis and rewiring, NIK is a driver of pathologies associated with metabolic dysfunction.

Introduction

Metabolic homeostasis relies on a balance between inputs such as glucose and oxygen necessary for energetic processes and utilization of catabolic pathways involving glycolysis and oxidative phosphorylation (OXPHOS) for efficient energy production [1,2]. Utilization of these major metabolic pathways is dynamic and shifts in response to alterations in cellular states or stress [3]. Glycolysis and OXPHOS are interwoven and dysregulation in one can alter the flux or rate of the other [4–6]. Although glycolysis yields low amounts of ATP its utilization is important for feeding into the TCA cycle and electron transport chain, for rapid production of ATP, or for cells under low oxygen availability [7–9]. Oxidative phosphorylation, or aerobic respiration, is more commonly utilized to meet ATP demands. Important to mitochondria respiration is the spare respiratory capacity (SRC) which is a measurable indicator of the efficiency of mitochondria to upregulate oxygen consumption to ramp up ATP production and meet changes in energetic demand [10–12]. As such, mitochondrial SRC is an important indicator of mitochondrial fitness and the ability of a cell to adapt to bioenergetic stress.

Metabolic syndrome is becoming increasingly common through a dysregulation in metabolic homeostasis. Typically, due to an excess energy intake, metabolic syndrome is characterized by inflammation, insulin resistance, hyperglycemia, lipodystrophy, and obesity. Adipose tissue is an essential organ to assist in this maintenance of metabolic homeostasis [13–15]. Through lipogenesis, adipose tissue acts as a reservoir for glycerol and excess fatty acids, then by lipolysis this organ supplies important fuel for glycolytic and mitochondria respiratory processes to meet energetic demands[16]. Adipose tissue is also a critical organ that is both effected by and attributes to metabolic syndrome. During states of energy excess, such as with diet-induced obesity, adipose tissue depots retain more lipid, increasing local inflammation, which then induces insulin resistance, contributing to a state of hyperglycemia and lipodystrophy [17,18].

Nuclear Factor-κB (NF-κB)-inducing kinase (NIK) is a serine, threonine protein kinase that is essential for activation of the noncanonical NF-κB pathway. NIK phosphorylates Inhibitor of κB-kinase-α (IKKα), to trigger p100 processing to p52 and generation of transcriptionally active p52-RelB complexes [19–22]. As an activator of a conserved immune pathway, NIK has been documented to have critical roles in B-cell, lymphocyte, and lymph node development, along with other immune functions such as immunoglobulin production and T-cell function [19,23–27]. Furthermore, more studies have highlighted important NF-κB-independent metabolic functions for NIK including roles in mitochondrial dynamics, metabolic reprograming under nutrient stress in cancer cells, as well as regulation of glycolysis in T-cells [28–30]. In response to diet-induced obesity, NIK has been demonstrated to regulate hyperglycemia by increasing glucagon activity and liver steatosis through induction of fatty acid oxidation [31–33]. Interest in understanding immune regulation of metabolic processes, such as in states of immunodeficiency, has considerably increased in recent years.

Here we investigate, a functional and developmental role for NIK in influencing metabolic homeostasis, highlighting regulation of adiposity and mitochondria respiration through SRC and proton leak. We specifically illustrate how NIK deficiency decreases overall adiposity and, in a noncanonical NF-κB-independent manner, mitochondria SRC. NIK deficient cells and tissue work at higher oxygen consumption rates (OCR) to increase basal rates of OXPHOS. This phenotype is accompanied by a significant increase in glycolytic activity in both *in vitro* and *ex vivo* data. Consistent with changes in metabolism, NIK deficiency also inhibits adipocyte differentiation in a noncanonical NF-κB-dependent manner through regulation of key adipogenic transcription factors. Strikingly, taken together, NIK deficiency protects mice from developing metabolic syndrome under a high-fat diet model, as NIK KO mice remain leaner, have increased insulin sensitivity, and higher glucose uptake.

Results

NIK KO Mice Display a Reduction in Overall Fat Mass

Analysis of gonadal white adipose tissue (gWAT) revealed that visceral deposits were substantially reduced in male and female NIK KO mice compared to WT and HET mice (Figure 1A,B, Supp. Figure 1A). Subcutaneous adipose was also observed to be reduced in NIK KO inguinal depots (ingWAT) (Supp. Figure 1B). Consistent with individual fat depot analysis, whole body composition assessment of live animals using EchoMRI™, demonstrated that male and female NIK KO mice had significantly less total fat mass, coupled with a higher lean mass ratio relative to body weight (Figure 1C,D). Moreover, while WT mice exhibited an increase in fat mass as they aged from 2 to 4 months, NIK KO mice maintained a reduced fat mass ratio (Figure 1E, Supp. Figure 1C,D). Although NIK KO mice gained less fat, they did not consume less food or water, nor were they more physically active than their littermates. On the contrary NIK KO mice ate and drank more than their WT littermates (Supp. Figure 2A-C). Also, NIK KO mice did not significantly differ in weight compared to WT mice until 15 weeks of age in males (Figure 1F), at which point the rate of fat mass development in WT mice surpassed the rate of body growth and adipose development of NIK KO mice. While adipocyte size was observed to be heterogeneous in NIK KO mice, they were generally smaller compared to WT mice, particularly in male mice (Figure 1G,H). This reduction in adipocyte size is to a lesser extent than the overall reduction in adipose mass, suggesting that the observed reduction in adiposity in NIK KO mice is due to a decrease in both adipocyte size and number (Figure 1H,I). Having observed reductions in adipocyte size and adipose mass, livers were examined for exogenous lipid accumulation which can occur due to defects in adipocyte function [34,35]. Oil Red O staining of liver sections revealed no differences in lipid accumulation between WT and NIK KO mice (Supp. Figure 2D). Taken together, these data suggest a role for NIK in the development of adipose tissue *in vivo*.

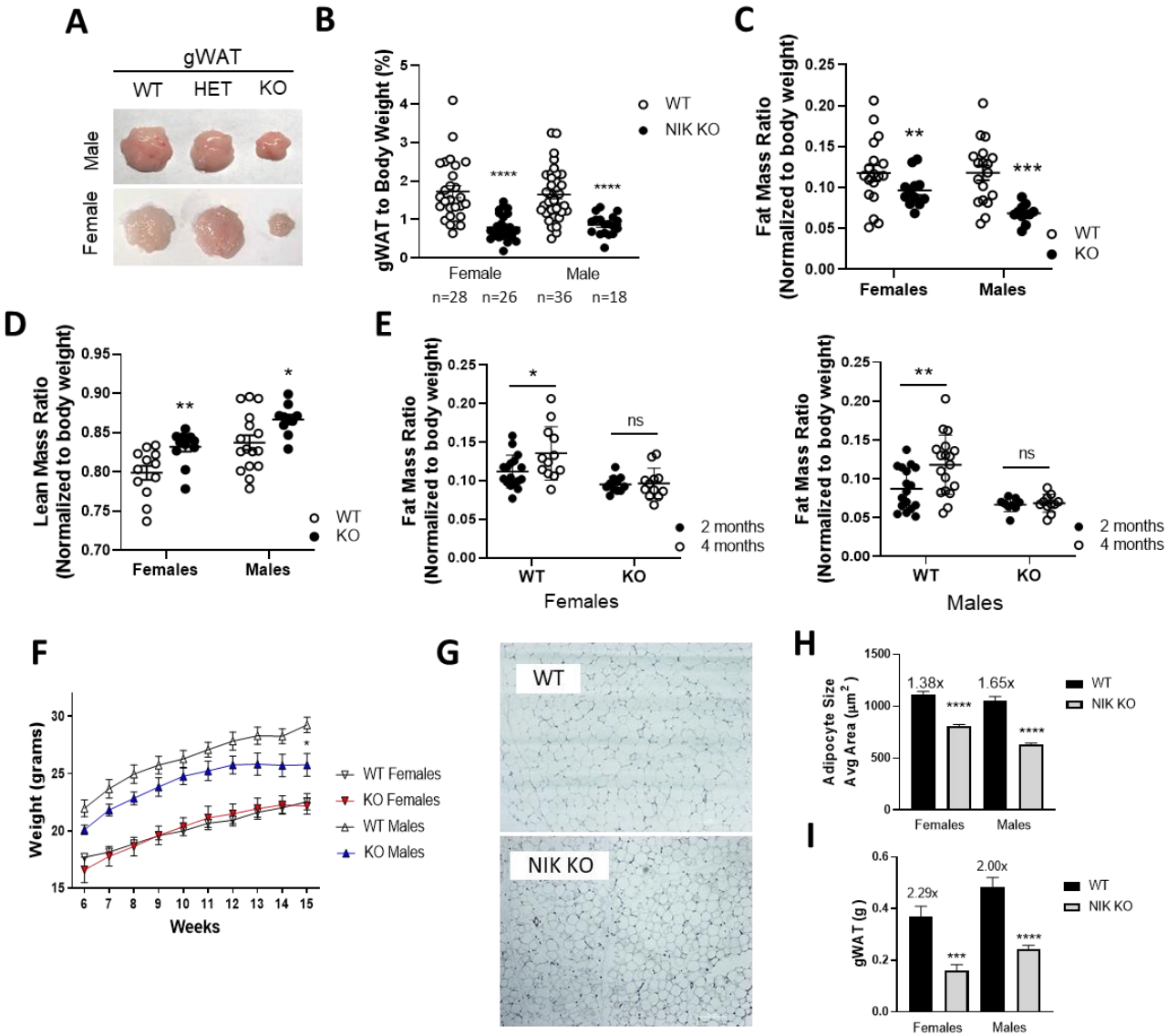

Figure 1: NIK KO Mice Display a Reduction in Overall Fat Mass

(A) Gonadal adipose tissue from male or female *Map3k14* littermates at 4 months of age. **(B)** Weight of gonadal fat between WT and NIK KO male and female *Map3k14* mice normalized to mouse weight. Data are represented as mean ± SD, Unpaired Student t-test. **(C)** EchoMRI™ measurements of overall fat and **(D)** lean mass of 4-month-old male and female mice normalized to body weight (Female *Map3k14* mice; WT n= 12 and KO n=12, Male *Map3k14*

mice; WT n=17 and KO n=10. Data represented at mean ± SEM, Unpaired Student t-test). **(E)** Fat mass ratio from body composition data of WT and NIK KO mice at 2 and 4 months of age. (Female *Map3k14* mice; WT at 2 months n=17, WT at 4 months n=12, KO at 2 months n=11 and KO at 4 months n=12. Male *Map3k14* mice; WT at 2 months n=17, WT at 4 months n=18, KO at 2 months n=9 and KO at 4 months n=11. Data represented at mean ± SD, Sidak's Multiple Comparisons Test). **(F)** Average weights of WT and NIK KO mice between males and females from 6-15 weeks (Female *Map3k14* mice; WT n= 9 and KO n=7, Male *Map3k14* mice; WT n=6 and KO n=5). Data represented at mean ± SEM, Sidak's Multiple Comparisons Test. **(G)** Hematoxylin and Eosin staining of gonadal white adipose tissue from WT and NIK KO female mice. **(H)** Image J quantification of the gonadal histology comparing adipocyte size between WT and NIK KO mice. For Females WT n=713 cells and NIK KO n=884; Males WT n=544 cells and NIK KO n=1007 cells, all across 3 mice each. **(I)** Weight of gonadal fat between WT and NIK KO male and female *Map3k14* mice. Data represented as mean ± SEM **(H,I)** Unpaired Student t-test.

NIK Regulates Mitochondria Efficiency and Metabolic Activity

We previously demonstrated that NIK regulates mitochondrial dynamics in glioblastoma cells by promoting mitochondria fission [29]. Similarly, C3H10T1/2 cells, a multipotent stem cell line capable of differentiating into adipocytes, exhibited larger, more fused mitochondria in the absence of NIK (Figure 2A,B), suggesting that NIK also regulates mitochondrial dynamics in adipocyte precursor cell lines. Given the reduction in adipocyte size and changes in mitochondria morphology in NIK KO cells, we sought to determine whether adipocyte metabolism was also altered in absence of NIK. Compared to WT cells, preadipocytes lacking NIK (3T3-L1 NIK-KO) displayed increased basal oxygen consumption rate (OCR) and ATP production. NIK KO cells exhibited an even more striking reduction of mitochondrial spare

respiratory capacity (SRC), which is the difference between basal and maximal respiration rates and an indicator of mitochondrial fitness. Additionally, NIK KO cells also displayed an increase in the proton leak, quantified by the OCR rate after oligomycin treatment. Ectopic expression of human wild-type NIK in NIK KO cells (NIK KO-hNIK) restored OCR and SRC, demonstrating that the observed mitochondrial defects are NIK-dependent. NIK-dependent regulation of OXPHOS does not require noncanonical NF-κB signaling, as cells lacking RelB, which is activated downstream of NIK, do not have impaired OCR/SRC (Figure 2C). Overall, these data indicate that mitochondria in cells lacking NIK are functional and more oxidative, consistent with their fused phenotype, but are incapable of efficiently upregulating OXPHOS to meet changes in energy demand.

Next, we evaluated whether NIK regulates glycolysis in addition to OXPHOS in preadipocytes. Similar to OCR, 3T3-L1 NIK KO cells exhibited significantly higher basal extracellular acidification rate (ECAR). NIK KO cells also exhibited the most robust increase in glycolysis after glucose treatment. Further analysis of the glycolytic stress test highlighted a higher capacity in 3T3-L1 NIK KO cells to upregulate glycolysis with considerable increases in maximum glycolytic rate, glycolytic capacity, and glycolytic reserve (Figure 2D). Together, our results demonstrated that while preadipocytes lacking NIK have decreased mitochondrial SRC, overall, they exhibit a significantly higher metabolic demand, with increased glycolysis and basal OXPHOS.

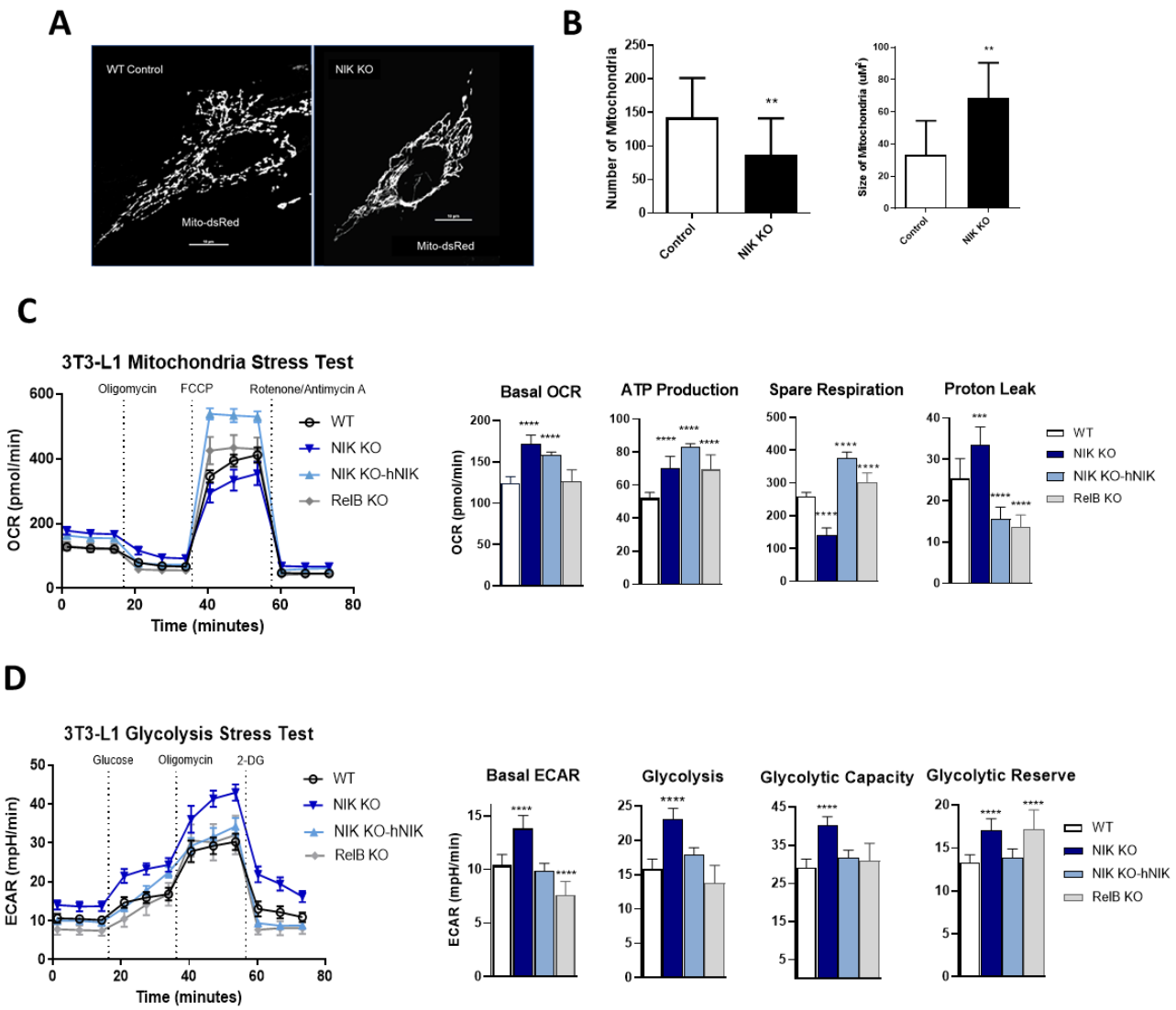

Figure 2: NIK Regulates Mitochondria Efficiency and Metabolic Activity

(A) C3H10T1/2, mouse stem cells, transfected and stained with Mito-dsRed. **(B)** Image J quantification of Mito-dsRed transfected WT and NIK KO C3H10T1/2 cells. Data represented as mean ± SD, Unpaired Student t-test. **(C)** Seahorse extracellular flux analysis of 3T3-L1 preadipocytes with either oxidative stress test (Mitochondria Stress Test) or with **(D)** Glycolysis Stress Test. **(C,D)** Data represented as mean ± SEM, Unpaired Student t-test.

Metabolic Demand Increases in NIK KO Adipose Tissue

In order to determine if the metabolic differences observed in NIK KO preadipocytes were translational to NIK KO mice, we analyzed OXPHOS and glycolytic rates on *ex vivo* adipose tissue. Similar to *in vitro* data, NIK KO adipose tissue samples displayed higher basal OCR rates and ATP production. Both NIK KO adipose tissue types also displayed a decrease in SRC and an increase in proton leak, with greater differences seen in the inguinal adipose depot than the gonadal. (Figure 3A). More characteristic of the metabolic phenotype with the loss of NIK is the robust increase in glycolysis which is emulated between both adipose types (Figure 3B). Extracellular flux analysis between both *in vitro* and *ex vivo* samples clearly demonstrated an increase in energetic demand with the loss of NIK, resulting in higher metabolic rates, more so with glycolysis. Total ATP measurements also indicated higher energy output from NIK KO inguinal WAT, about 1.5x more than WT, and similar ATP levels in the gonadal WAT compared to WT (Figure 3C). Related to the considerable increase in glycolysis, we also saw an increase in glucose uptake in the NIK KO adipose tissue with ingWAT and gWAT being 1.4x and 1.3x higher than WT respectively (Figure 3D). NIK KO tissue also responded to the β-agonist and lipolytic stimulant, isoproterenol, more so in the gWAT compared to WT, indicating functional adipocytes with an ability for lipid turnover (Figure 3E). Overall, *in vitro* and *ex vivo* data with the loss of NIK display similar metabolic dynamics, exhibiting a higher energy demand with a greater increase in glycolysis, and a regulation of mitochondria function through SRC and proton leak by noncanonical NF-κB-independent roles.

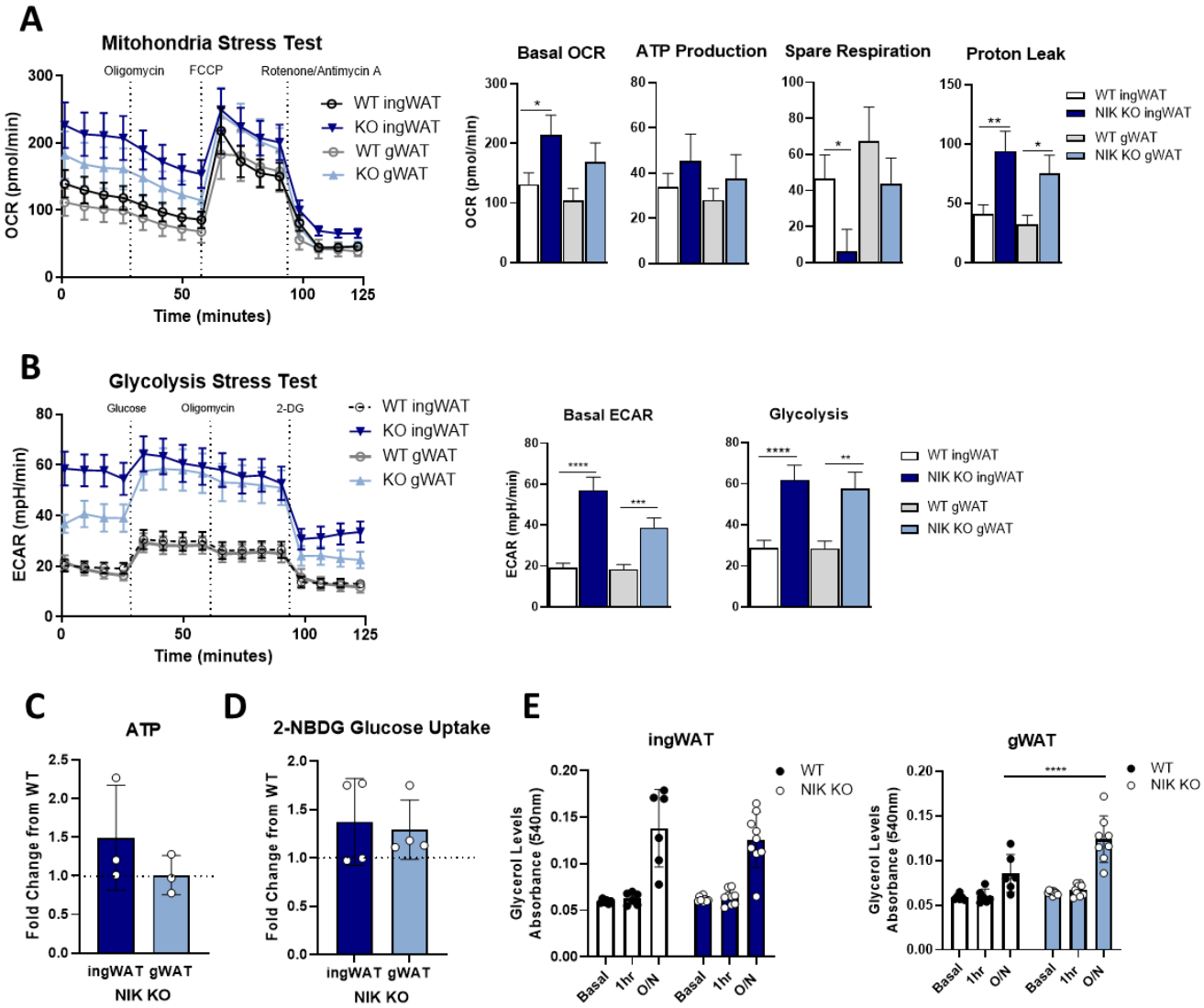

Figure 3: Metabolic Demand Increases in NIK KO Adipose Tissue

(A) Seahorse extracellular flux analysis of *ex vivo* mouse gonadal or inguinal WAT with either oxidative stress test (Mitochondria Stress Test) or with **(B)** Glycolysis Stress Test. **(A,B)** WT n=5, NIK KO n=4, male mice. **(C)** Overall ATP analysis of mouse gonadal or inguinal WAT by luminescence. NIK KO tissue fold change compared to WT tissue. WT base line represented at 1. Data represented as mean ± SEM, Unpaired Student t-test. **(D)** Analysis of glucose uptake by fluorescent 2-NBDG of mouse gonadal or inguinal WAT. NIK KO tissue fold change compared

to WT tissue. WT base line represented at 1. **(E)** Glycerol levels of gonadal or inguinal WAT with lipolysis stimulated with isoproterenol and measured at 1 hour and then after overnight incubation. Sidak's Multiple Comparison Test. **(C-E)** Data represented as mean ± SD.

NIK KO Mice Exhibit Systemic Sex Specific Metabolic Differences

With observed differences in cellular and whole tissue analysis with the loss of NIK, we then examined NIK KO mice for systemic differences in metabolism. Whole body metabolism was measured across light and dark cycles using metabolic cages to analyze respiratory rates and energy expenditure of individual mice along with feed and water intake and activity. Overall, female NIK KO mice displayed a higher oxygen consumption and carbon dioxide production rate throughout both periods of the day, than their WT counterparts, while NIK KO males displayed rates similar to WT (Figure 4 A, B). Consequentially, the changes in respiratory rates generate a higher trend in the respiratory exchange rate for NIK KO mice, indicative of greater glucose oxidation over fatty acid oxidation (Figure 4C) [36]. Moreover, this data revealed that NIK KO mice at 4 months of age displayed a higher overall energy expenditure, exhibited more so in females than males (Figure 4D). In addition to increased metabolic outputs, NIK KO mice also maintained higher temperatures at 2 months of age, with female mice maintaining elevated temperatures as seen at 4 months (Figure 4E,F). While male mice displayed adipose specific increases in metabolism from extracellular flux analysis, only female mice exhibited systemic differences. This trend for an overall increase in whole body metabolic activity in the NIK KO mice is observable in aging mice, indicating a potential for compounding immune development effects on systemic metabolism (Supp. Figure 3).

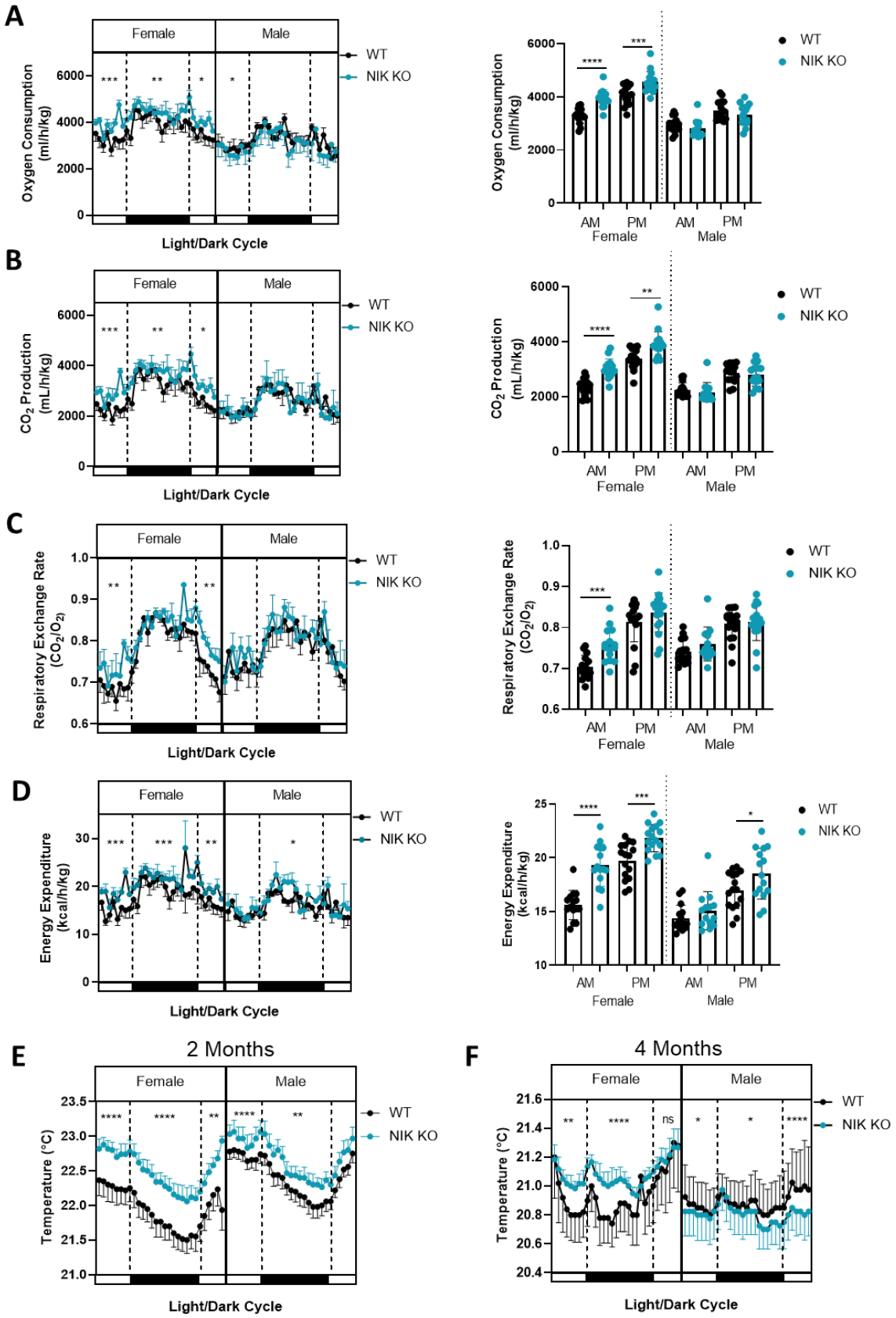
A
Female
Male
WT
NIK KO
Oxygen Consumption (ml/h/kg)
Light/Dark Cycle
AM
PM
Female
Male
B
CO2 Production (mL/h/kg)
C
Respiratory Exchange Rate (CO2/O2)
D
Energy Expenditure (kcal/h/kg)
E
2 Months
Temperature (°C)
F
4 Months
ns

240

Figure 4: NIK KO Mice Exhibit Systemic Sex Specific Metabolic Differences

(A-D) Data collected from 4-month-old male and female *Map3k14* mice individually housed in metabolic cages. Morning and night analysis from a 24-hour time period of **(A)** oxygen consumption, **(B)** CO_2 production, **(C)** respiratory exchange rate (CO_2/ O_2), and **(D)** caloric energy expenditure **(E)** cage temperature with mice at 2 months of age and at **(F)** 4 months of age. Line graphs represented as mean ± SEM, bar graphs represented as mean ± SD. **(A-D,F)** Females WT n=5, NIK KO n=6; Males WT n=4, NIK KO n=3. **(E)** Females WT n=6, NIK KO n=5; Males WT n= 5, NIK KO n=3.

A Role for Noncanonical NF-κB-Dependent Signaling in Promoting Adiposity

Given the reduction in NIK KO adipose tissue was due to a reduction in adipocyte size and number, we utilized C3H10T1/2 and 3T3-L1 cells to investigate changes in adipogenic potential with the loss of NIK. Strikingly, NIK KO cells were severely impaired in their ability to form mature adipocytes, as demonstrated by staining of lipid droplets that form in mature adipocytes. Expression of a wild-type human NIK construct in NIK KO cells (NIK KO-hNIK) restored adipogenesis to the same extent as control cells, confirming the crucial role of NIK in adipocyte development (Figure 5A, Supp. Figure 4A,B). Importantly, primary bone marrow-derived stem cells isolated from NIK KO mice were also impaired in their ability to differentiate into mature adipocytes compared to MSCs isolated from WT mice (Supp. Figure 4C). Furthermore, treatment of WT cells with a NIK specific inhibitor, B022, impeded adipocyte differentiation similar to cells lacking NIK (Supp. Figure 4D,E) [37].

To evaluate if the effects the loss of NIK had on adipogenesis were dependent on NF-κB, we analyzed adipogenic differentiation of 3T3-L1 cells with genetic modifications of NF-κB proteins. RelB KO cells mimicked NIK KO cells and exhibited impaired adipocyte differentiation.

Moreover, overexpression of IKKα and RelB in NIK KO cells (NIK KO-IKKα, NIK KO-RelB) substantially rescued adipocyte differentiation similar to the re-expression of NIK (NIK KO-hNIK). In contrast, overexpression of RelA, a canonical NF-κB transcription factor, in NIK KO or RelB KO cells was unable to restore adipocyte differentiation, and the loss of RelA did not impair adipogenesis (Figure 5B, Supp. Figure 5A). In addition to the observed effects of altered NF-κB expression on adipogenesis, immunoblot assays further demonstrated that transcription factor activation and induction of the canonical NF-κB pathway (p-RelA-S536) decreased significantly by 4-6 days after induction of adipocyte differentiation. Conversely, expression of the noncanonical NF-κB protein RelB, increased throughout adipocyte differentiation (Supp. Figure 5B). Furthermore, activation of the canonical NF-κB pathway with TNFα inhibited adipocyte differentiation in WT C3H10T1/2 cells, whereas preferential activation of the noncanonical NF-κB pathway with TWEAK did not inhibit adipogenesis (Supp. Figure 5C,D). These findings indicate that NIK promotes adipocyte differentiation through the noncanonical NF-κB pathway, while the canonical NF-κB pathway maintains an inhibitory effect.

Interestingly, NIK and RelB were required for the induction of the essential adipogenic transcription factors PPARγ and one of its targets, C/EBPα [38] (Figure 5C, Supp. Figure 5E). Ectopic expression of NIK or RelB rescued the ability of NIK KO cells to respond to the PPARγ agonist ETYA (eicosatetraynoic acid), and increased PPARγ and C/EBPα expression (Figure 5D, Supp. Figure 5F). PPARγ was also observed to be decreased in NIK KO liver extracts (Supp. Figure 5G). In addition to lower expression of PPARγ, expression of the PPARγ-regulated, adipocyte-specific genes adiponectin (*ADIPOQ*), glucose transporter 4 (GLUT4, *SLC2A4*), and glycerol-3-phosphate dehydrogenase (*GPD1*), were significantly impaired in NIK KO and RelB KO cells even when treated with a PPARγ agonist. The ability of these cells to induce PPARγ activity and increase adipogenic genes to form functional adipocytes was restored by re-expression of NIK or RelB (Figure 5E). Additionally, the overexpression of

PPARγ or C/EBPα rescued adipocyte differentiation in NIK KO C3H10T1/2 and 3T3-L1 cells, further demonstrating that the deficiency for NIK KO cells to undergo adipogenesis lies in their inability to increase levels of these key adipogenic transcription factors (Figure 5F). These data suggest that NIK and the noncanonical NF-κB pathway are required for regulating the expression and activity of PPARγ and C/EBPα to promote adipogenesis.

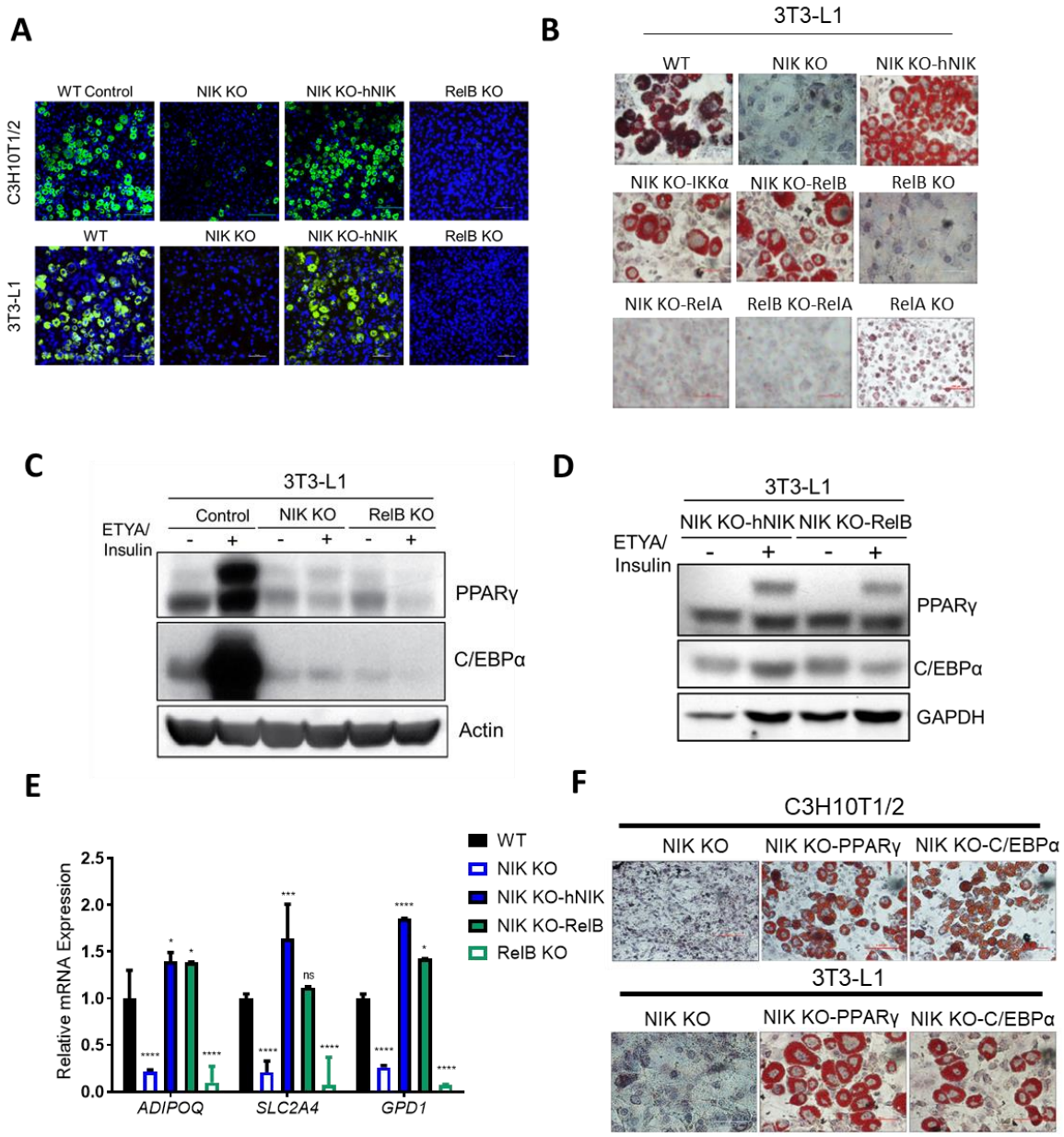

Figure 5: A Role for Noncanonical NF-κB-Dependent Signaling in Promoting Adiposity

(A) Fluorescent BODIPY lipid staining of C3H10T1/2 and 3T3-L1 cells showing a significant reduction in adipogenesis with the loss of NIK which is rescued in NIK KO-hNIK cells. **(B)** Oil Red O staining of differentiated 3T3-L1 cells lacking or over expressing various noncanonical/canonical NF-κB proteins. **(C)** PPARγ and C/EBPα expression in undifferentiated vs adipogenic treated in NIK KO and RelB KO 3T3-L1 cells compared to WT control cells. **(D)** PPARγ and C/EBPα expression in undifferentiated vs adipogenic treated 3T3-L1 cells with re-expression of human NIK or overexpression of RelB in NIK KO cells (NIK KO-hNIK, NIK KO-RelB). **(E)** qPCR analysis of adipocyte genes (*ADIPOQ, SLC2A4, GPD1*) in ETYA/insulin treated C3H10T1/2 cells. Data represented as mean ± SD, Tukey's Multiple Comparison Test. **(F)** Oil Red O staining of differentiated NIK KO or NIK KO with overexpression of PPARγ or C/EBPα in C3H10T1/2 and 3T3-L1 cells.

NIK Regulates Susceptibility to Diet-Induced Obesity

Having observed the effects of NIK on adiposity, metabolism, and adipogenesis we next sought to investigate if NIK played a role in adipose tissue expansion in response to a high-fat diet (HFD). After 2-3 months on a HFD both male and female NIK KO mice showed significantly less weight gain than their wild-type counterparts (Figure 6A,B). Specifically, NIK KO mice exhibited a 50% decrease in gWAT tissue compared to mice (Figure 6C). Under a HFD male and female NIK KO mice also displayed a reduction in the subcutaneous depot (ingWAT) compared to WT littermates (Figure 6D). In addition to a significant reduction in fat mass, *ex vivo* analysis of gonadal adipose tissue revealed that similar to mice on a chow diet, NIK KO mice on a HFD exhibited smaller adipocytes (Figure 6E, F). However, the decrease in adipocyte size was to a lesser extent than the overall reduction in gWAT mass (Figure 6F, G). Therefore,

the reduction in NIK KO adipose tissue is likely due to a decrease in both adipocyte size and number. Whole body composition analysis demonstrated that on a HFD, NIK KO mice maintained a lower fat mass overall and a higher lean mass ratio by body weight compared to WT mice (Figure 6H). Notably, NIK KO mice gained about 3x less fat than WT mice on a HFD compared with standard chow (Figure 6I). In addition to maintaining a reduction in adiposity, glucose tolerance testing demonstrated that NIK KO mice were more efficient at clearing glucose than WT littermates, suggesting an increase in insulin sensitivity (Figure 6J). This was confirmed with insulin tolerance testing where NIK KO mice cleared glucose more rapidly than WT mice after an administration of insulin (Figure 6K). Analysis of adipogenic genes from the inguinal WAT of HFD mice also revealed a reduction in fatty acid binding protein 4 (*FABP4*; Ap2), and an increase in GLUT4 and *GPD1* (Supp. Figure 6A,B). Increased GLUT4 gene expression complements both an increase in glucose clearance of NIK KO mice and higher glycolytic demands of NIK KO adipose tissue. Further evidence supports the uptake of glucose by the whole mouse to fuel glycolytic demands as gene expression for glycogen synthase is significantly down regulated in NIK KO livers and thus glucose is not being stored (Supp. Figure 6C,D). Reduction in lipid storage of NIK KO adipocytes does not seem to be associated with adipocyte dysfunction as NIK KO mice do not have exogenous lipid storage in their livers even on a HFD as seen by Oil Red O staining. This lipid reduction is accompanied by lower gene expression of fatty acid binding protein (*FABP1*) and fatty acid oxidation genes (*MCAD, CPT1α*) (Supp. Figure 6D,E). Overall, the data show NIK has a previously unrecognized role in mediation of adipocyte development and adipose expansion, with its inhibition acting as a preventative of metabolic disorders including diet-induced obesity and diabetes.

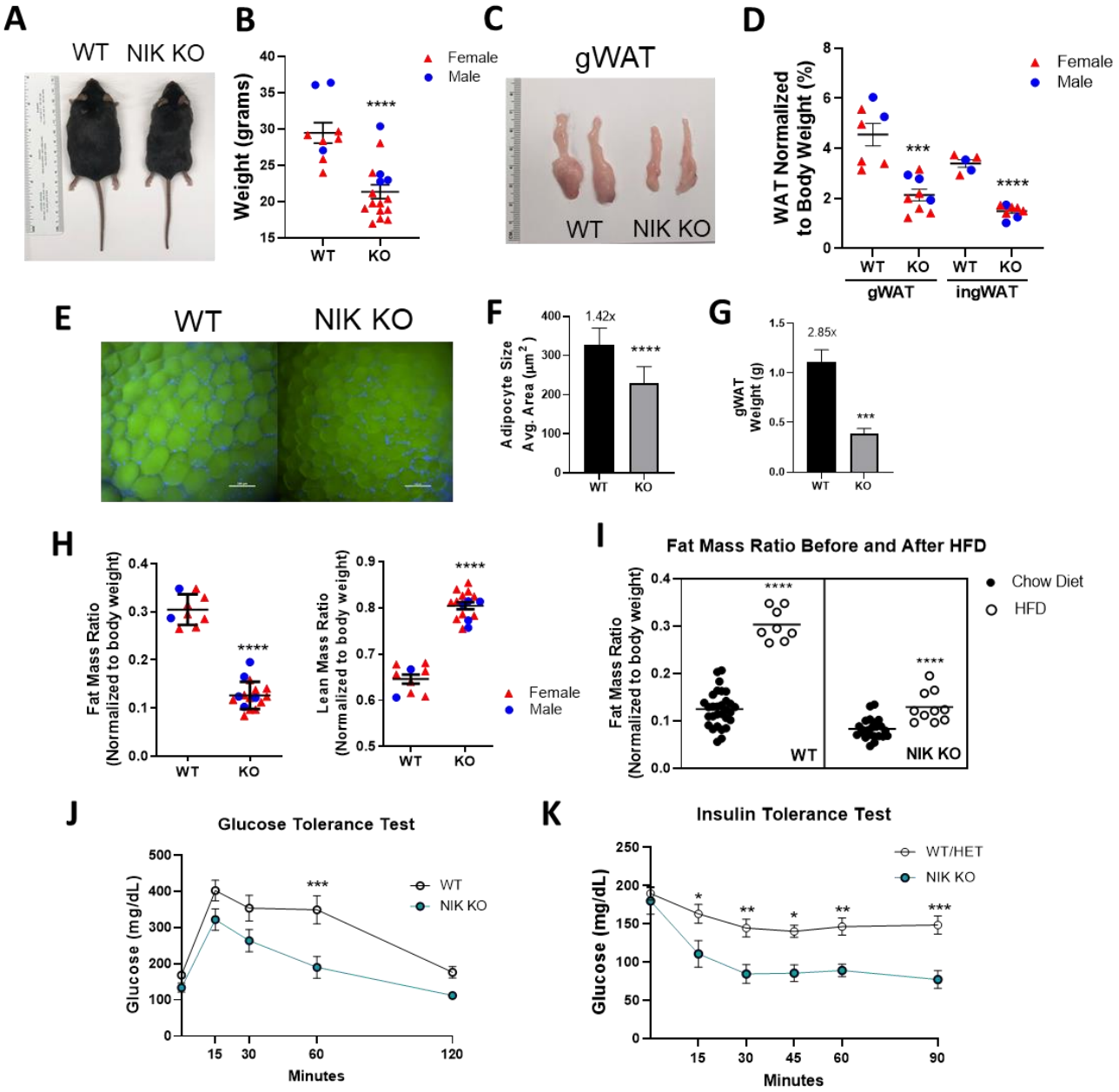

Figure 6: NIK Regulates Susceptibility to Diet-Induced Obesity

(A) Images of male WT and NIK KO mice on HFD. **(B)** Weights of WT and NIK KO male and female mice exposed to a HFD for about 3 months (mice exposed to a HFD in utero up until weaning and then 8-10 weeks after weaning). Data represented as mean ± SEM, Unpaired Student t-test. **(C)** Gonadal white adipose tissue from male mice on a HFD. **(D)** Weights of

gonadal and inguinal white adipose tissue from male and female mice normalized to body weight. Data represented as mean ± SEM, Unpaired Student t-test. **(E)** Whole mount staining of gonadal white adipose tissue from WT and NIK KO female mice on a HFD with BODIPY (green) and Hoechst (blue). **(F)** Image J quantification of adipocyte size from female mice on a HFD for about 10 weeks. Data represented as mean ± SD, WT n=100 cells from 5 different images across 3 different mice and NIK KO n=120 cells from 6 different images across 3 different mice. **(G)** Weights of gonadal adipose tissue from female WT and NIK KO mice on HFD. **(H)** EchoMRI™ data of fat and lean mass from female and male WT and NIK KO mice on a HFD normalized to weight. Data represented as mean ± SEM, Unpaired Student t-test. **(I)** Fat mass data from EchoMRI™ analysis comparing fat mass ratios from a chow diet to a HFD between WT and NIK KO mice. **(J)** Glucose tolerance test on WT and NIK KO mice on a HFD. Data represented at mean ± SEM, Sidak's Multiple Comparisons Test. WT n=8, NIK KO n=12. **(K)** Insulin tolerance test on WT, HET and NIK KO mice on a HFD. Data represented at mean ± SEM, Sidak's Multiple Comparisons Test. WT/HET n=10, NIK KO n=6.

Discussion

Maintenance of energy balance is critical for the normal function of physiological processes and is a potent indicator of health status. In this study, we demonstrate for the first time that mice lacking NIK exhibit higher metabolic output and energy expenditure resulting in decreased adiposity and increased resistance to obesity. NIK KO mice maintained a leaner deposition, even under a high-fat diet, despite their decreased physical activity and increased eating (see Figs. 1 & 6 and Supp. Figs. 2 & 3). Consistent with these *in vivo* findings, *in vitro* and *ex vivo* analysis revealed that aerobic respiration and glycolysis are elevated in NIK KO preadipocytes and adipose tissue. However, NIK KO preadipocytes and tissue also exhibited significantly impaired spare respiratory capacity and elevated proton leak, suggesting that in the

absence of NIK, mitochondria work at higher, but inefficient, metabolic rates while triggering a compensatory upregulation of glycolysis (see Figs. 2 & 3). This compensatory upregulation of aerobic glycolysis has parallels to the Warburg effect in cancer cells[39], which has been hypothesized facilitate rapid generation of ATP using glucose as carbon source for anabolic pathways, while controlling ROS production and redox homeostasis [40].

While NIK KO mice overall exhibited a reduced adipose phenotype and *in vitro* and *ex vivo* data demonstrated changes in metabolic demands with the loss of NIK, only females exhibited whole body metabolic changes, including increased energy expenditure and temperature (see Fig. 4). Observed elevated thermogenesis may be a result of increased mitochondria proton uncoupling which is consistent with the higher proton leak observed in NIK KO cells. These sex differences could be attributed to distinct metabolic or immune changes between genders. For example, although females are more apt to adipose deposition than males, estrogen increases insulin sensitivity and protects female mice from diet-induced obesity [41–43]. Furthermore, there are known sex differences in the development and function of immunity between genders that could have systemic metabolic effects [44]. In this context, ablation of NIK increases susceptibility to viral and bacterial infections, consistent with well-established roles for NIK in regulating immunity[19,23]. Changes in bacterial flora or viral infection have been shown to alter host metabolism in order to support replication [45,46]. Furthermore, as a regulator of immune cell development, the loss of NIK can have effects on the metabolic status and recruitment of adipose tissue immune cells that can play critical roles in regulating tissue homeostasis. Nevertheless, we note that *in vitro* differentiated pre-adipocytes exhibited metabolic phenotypes similar to *ex vivo* adipose tissue (see Figs. 2 & 3), demonstrating that NIK has adipose cell-intrinsic metabolic functions. Use of a systemic knockout mouse model provided insight into the metabolic ramifications associated with NIK loss-of-function immunodeficiency.

Our findings also revealed opposing effects of canonical and noncanonical NF-κB signaling in regulating adipogenesis (see Fig. 5 and Supp. Fig. 5). These observations are

consistent with previous data showing that activation or overexpression of the canonical NF-κB/RelA pathway inhibits adipogenesis, and that RelA itself is inhibited by adipogenic-promoting PPARγ agonists *in vitro* and *in vivo* [47,48]. Additionally, an increase of RelB and p52 during adipocyte differentiation was similarly seen in a separate study analyzing 3T3-L1 cells [49]. However, a cooperative role for the canonical and noncanonical NF-κB pathways in promoting adipocyte differentiation was previously reported in a study of adipose-specific RelB knockout mice in response to lymphotoxin-β-receptor (LTβR) activation [50]. Additionally, a separate study demonstrated that mice with adipose-specific knockout of Tank-binding kinase 1 (TBK1), a repressor of NIK stability, exhibited a slight reduction in adipose tissue and adipocyte size under a prolonged HFD, which was accompanied by increased noncanonical, as well as canonical NF-κB signaling, which were linked to hyper-inflammation [51]. Our results suggest that there are likely signal-specific roles for RelB in regulating PPARγ expression and adipogenesis. Moreover, NIK may have RelB-independent, or non-cell autonomous effects on adipogenesis and adipose development. In the context of these findings, the signals responsible for activating NIK during adipocyte development and expansion under a HFD warrant further study.

A key finding reported here is our observation that NIK KO mice displayed increased resistance to HFD-induced obesity by maintaining reduced weight and overall fat mass (see Fig. 6). This phenotype was accompanied by increased metabolic fitness seen in the NIK KO mice with greater insulin sensitivity and glucose clearance than WT mice. Our data are consistent with a previous report demonstrating that NIK activity is increased in the livers of genetic (*ob/ob)* or HFD-fed obese mice, and liver-specific loss of NIK increases glucose metabolism [31,32]. Finally, we have established that NIK KO mice maintained smaller adipocytes even under a prolonged HFD (>1 month), and NIK KO primary mesenchymal stem cells exhibit reduced adipocyte differentiation (see Figs. 1 & 6 and Supp. Fig. 4). These results suggest that NIK mediates adipose hyperplasia as well as hypertrophy. Taken together, our data suggest that systemic NIK inhibition may have efficacy in treating or preventing metabolic syndrome caused

by diet-induced obesity through inhibition of hyperglycemia, insulin resistance and adipose tissue expansion, as well as increased metabolic output and energy expenditure.

Author Contributions: Conceptualization, K.M.P., D.W.L., R.S.; writing—original draft preparation, K.M.P., writing—review and editing, K.M.P. and R.S.; visualization: K.M.P., R.S.; funding acquisition: R.S.; supervision, R.S. All authors have read and agreed to the publication of the manuscript.

Funding: NIH-1R01NS082554 to R.S.

Acknowledgments: We thank Dr. Joseph M. Rutkowski for the contribution of the 3T3-L1 cells and critical review of the manuscript. We would also like to thank Dr. David Threadgill and his lab, including Dr. Alexandra Trott and Orion Hicks at the Texas A&M Rodent Preclinical Phenotyping Core, for assistance with the EchoMRI™ machine and TSE Phenomaster™ metabolic cages.

Conflicts of Interest: The authors declare no conflicts of interest.

Materials and Methods

Animal Procedures & Ex Vivo Work

All animal experiments were done in accordance with animal use protocol (2019-0102) with approved IACUC guidelines. *Map3k14* mice were purchased from Jackson lab (B6N.129-Map3k14tm1Rds/J) and maintained by heterozygous breeding.

Cell Culture

Mesenchymal stem cell line and preadipocyte cell line, C3H10T1/2 and 3T3-L1 were cultured in DMEM supplemented with 10% FBS, 100 U/ml penicillin and 0.1mg/ml streptomycin (Thermo Fisher Scientific, Waltham, MA). 293 T cells were obtained from ATCC (www.atcc.org) and cultured in DMEM supplemented with 10% FBS, 100 U/ml penicillin and 0.1mg/ml streptomycin. Bone marrow MSC cells were isolated from the femurs of mouse and cultured in DMEM supplemented with 10% FBS, 100 U/ml penicillin and 0.1mg/ml streptomycin**.**

Bone Marrow Cell Isolation

Mouse femurs are collected and sterilized in 70% ethanol and then were crushed in sterile PBS in a mortar with a pestle. From the crushed femurs, 5mL of DMEM (with 10% FBS and 1% penicillin/streptomycin) is then used to collected cells into a conical tube through a 70μM filter. Cells are then centrifuged at 1500rpm for 8 minutes. Media is removed and the cell pellet is resuspended in 3mL of ACK lysis buffer (Lonza 10-548E) for 2 minutes. ACK cell suspension is diluted with 10mL of media and pelleted again. The cell pellet is resuspended in 10mL of media and filtered through a 40μM filter.

CrispR-Cas9 Gene Knockout

NIK: Oligos encoding guide RNAs for murine NIK (gNIK- 1: AGGAUGGGGCAUUCCGCUGU gNIK-2: UACCUGGUGCAUGCGCUCCA, gNIK-3: AGUAUCGAGAAGAGGUCCAC) RelB: Oligos encoding guide RNAs for murine RelB (g RelB-1: AGCGGCCCUCGCACUCGUAG, gRelB-2: GCGCUUCCGCUACGAGUGCG, gRelB-3: ACUGCACGGACGGCGUCUGC) Each gRNAs were cloned into Lenti-CrispR-v2 (Addgene, Cambridge, MA) respectively. C3H10T1/2 and 3T3-L1 cells were transduced with a mixture of lentiviruses (described below) carrying the three murine gRNAs. Puromycin resistant single clonal cells were isolated by serial dilution and experiments were repeated with at least two clones. Loss of NIK or RelB expression was confirmed by immunoblot analysis. For controls, cells were transduced with empty LentiCrispR-V2.

Gene Overexpression

Lentiviral construct of over-expression constructs (NIK, IKKα, RelB, RelA, PPARγ and C/EBPα) was obtained from DNASU (Tempe, AZ).

Lentivirus Production

24μg of lentiviral plasmids and 72μg of polyethyleneimine (Sigma-Aldrich) were used to transfect 293T cells. After 3 days of transfection, viral supernatant was concentrated 20 fold to 500μl using Lenti-X Concentrator (Clontech, Mountain View, CA), and 100μl of concentrated virus was used to infect cells. Stably transduced cells were selected for 72hr in medium containing 0.6μg/ml puromycin or 6μg/ml blasticidin (Thermo Fisher).

Seahorse Extracellular Flux Analysis

3T3-L1 Cells

Metabolic activity was analyzed using a Seahorse XFe96 Analyzer (Agilent, Santa Clara, CA). For 3T3-L1 cells, forty-thousand cells per well were plated in the collagen-coated (40ng/µL) Agilent Seahorse XFe96 microplates and left to settle overnight before analysis. Mitochondrial Stress Tests were conducted according to the manufacturer's guidelines. Base media was supplemented with 25mM glucose (Sigma, G7021, St. Louis, MO), 2mM glutamine (Sigma, G85420, St. Louis, MO), and 1mM pyruvate (Gibco). Inhibitors were used at the following final concentrations (10x inhibitor was added to injection ports to reach final concentration): 1µM oligomycin A (Sigma, 75351, St. Louis, MO), 2µM FCCP (Sigma, C2920, St. Louis, MO), and mixture of 0.5µM rotenone (Enzo Life Sciences, Farmingdale, NY, ALX-350-360) and 0.5µM antimycin A (Sigma, A8674, St. Louis, MO).

For Glycolysis Stress Tests, cells were plated in a similar manner, but glucose-starved for 1hr in Seahorse DMEM base media with 2mM glutamine before analysis. Reagents for injections were used at the following final concentrations (10x reagent was added to injection ports to reach final concentration): 10mM glucose, 10uM oligomycin A, 50mM 2-DG (Thermo Fischer Scientific, 50-519-066).

After Seahorse analysis, DNA content was measured using DRAQ5 staining (Thermo Fisher Scientific, 50-712-282) for normalization. Assay was ran in 2 biological replicates with samples ran in 6-8 replicates per assay. Analyses were conducted using Seahorse Wave Controller Software v2.6 and XF Report Generators (Agilent Technologies).

***Ex Vivo* Adipose Tissue**

Analysis of metabolic activity of adipose tissue was adapted from PMID: 24529442 [52]. 96 well Seahorse plates were coated twice with Cell-Tak (50µg/mL, Corning® Cell-Tak™ Cell and Tissue Adhesive, Cat. No. 354240). Tissue was excised fresh, rinsed well in PBS, and cut into small, >1mg, pieces of similar size and plated into the center of the wells. For Mitochondria Stress Test, base media was supplemented with 25 mM glucose, 2 mM glutamine, and 1 mM

pyruvate. Inhibitors were used at the following final concentrations (10x inhibitor was added to injection ports to reach final concentration): 20μM oligomycin A, 20μM FCCP, and mixture of 20μM rotenone and 20μM antimycin A. Tissue samples are ran in 5 or more replicates per tissue type per assay. Well replicates with poor compound responses were eliminated from analyses.

For Glycolysis Stress Test base media was supplemented with 2mM glutamine, and reagents for injections were used at the following final concentrations (10x reagent was added to injection ports to reach final concentration): 25mM glucose, 20μM oligomycin A, 100mM 2-DG.

Run time for tissue was increased to 30 minutes per injection with four measurements per compound (4 cycles of 3 min mix, 1.5 min wait, 3 min measure). Afterwards, tissue was homogenized and lysed and normalized by protein.

Immunofluorescence

For immunofluorescence of C3H10T1/2 mitochondria staining, cells were transfected with 1μg DsRed2-Mito-7 (Addgene Plasmid #55838) by lipofectamine (Invitrogen L3000008) for 48-72hrs. Cells were then fixed with 4% PFA for 20 minutes at 37°C. After fixation, cells were washed twice with PBS and then stained with Hoechst (1:1000) diluted in 1% BSA, .1% Triton-X in PBS for 10 minutes. Cells were imaged by confocal (Nikon TI A1R inverted confocal microscope).

BODIPY Staining

For immunofluorescence imaging, BODIPY™ 490/509 (4,4-Difluoro-1,3,5,7,8-Pentamethyl-4-Bora-3a,4a-Diaza-s-Indacene) (Sigma Aldrich 790389) was used. 5mM of BODIPY dye was diluted 1:2500 in PBS and incubate on live cells for 10 minutes at 37°C. Afterwards, cells were washed twice with PBS and then fixed in 4% PFA for 20 minutes at 37°C. After fixation, cells

were washed twice with PBS and then stained with Hoechst (1:1000) diluted in 1% BSA, .1% Triton-X in PBS for 10 minutes. Cells were imaged by confocal (Nikon TI A1R inverted confocal microscope).

ATPlite

Tissue was normalized by weight (5mg) and ran in triplicate. Tissue was lysed using kit reagents, following manufacture guidelines (Perkin Elmer, 6016941). Lysates were measured for luminescence. Knockout was normalized to respective wild-type sample per run for fold change.

2-NBDG Uptake

Small pieces of tissue (about 2-5mg) were cut from subcutaneous and gonadal WAT and placed in a 96well plate in duplicate or triplicate with 300µg/mL2-NBDG (Cayman, 11046) (enough to cover tissue, about 50-100µL). Tissue was then incubated at 37°C for 1 hour. Afterwards, tissue was washed with PBS 2x and then lysed. Supernatant was then analyzed by plate reader for 2-NBDG (455-570nm). Fluorescent readouts are normalized to protein content.

Lipolysis

About 2-5mg was placed in a 12 well plate in duplicate or triplicate. Tissue was left to sit in 300µL DMEM without FBS for an hour in the incubator. Media was removed for t=0 and isoproterenol was added for a final concentration of 100µM. Tissue was incubated with the isoproterenol for an hour and then media was removed for t=1 timepoint, final samples were taken after overnight incubation. 10µL of each sample at the different points were mixed with160µL of glycerol reagent (Sigma, F6428) and read at an absorbance of 540nm for glycerol levels.

Adipocyte Differentiation

Adipocyte differentiation was induced by treating confluent cells for 2 days with 5 μg/ml insulin (Thermo Fisher Scientific) and 10μM ETYA (Santa Cruz Biotech, Dallas, TX) in Dulbecco's modified Eagle's medium containing 10% FBS, and then every 2 days for 6 Days with insulin (5 μg/ml).

Treatment with NIK inhibitor B022 was purchased from MEDCHEM EXPRESS (Cat. No. HY-120501) and used at a concentration of 5μM.

TNFα (ProSpec CYT-223) and TWEAK (PeproTech 31006) were used at 10ng/mL.

Oil Red O Staining

For the Oil Red O staining, Oil Red O staining solution (0.5% Oil-Red O in isopropyl alcohol solution-distilled water [60:40]) was filtered through the Whatman no. 1 filter paper. Cells were fixed with 10% formaldehyde solution for 30 min at 37°C, then washed with 60% isopropyl alcohol followed by staining with the filtered Oil Red O solution for 20 min and then washed with distilled water three times.

To measure Oil Red O staining of adipocyte differentiated cells, dye is eluted with 100% isopropanol for 10 minutes. Eluted dye is transferred to 96 well plate and optical density measurements were done on Perkin Elmer plate reader at 500nm, .5 sec.

Immunoblot

Cells were lysed in RIPA lysis buffer (Thermo Fisher Scientific) with protease/phosphatase inhibitor cocktail (Thermo Fisher Scientific). Protein was mixed with NuPage 4X LDS sample buffer (Thermo Fisher Scientific) containing reducing agent and denatured at 100˚C for 7 min. Proteins were separated on 8% ~ 12% SDS-PAGE and transferred to nitrocellulose membranes

(Amersham). The membranes were blocked for 1h with 5% non-fat dry milk in 0.1% Tween-20/TBS (TBST) and incubated with primary antibodies diluted in blocking buffer at 4°C overnight. After washing in TBST, membranes were incubated with secondary in BSA for 1 hour at room temperature. The blots were washed with TBST and developed using Chemiluminescent HRP Substrate (EMD Millipore) for detection of HRP or an Odyssey Infrared Imaging system (LI-COR Biosciences) for detection of IRDye fluorescent dyes.

Antibodies

Following antibodies were used C/EBPα: CST8178 (Cell Signaling Technology), GPD1 (sc-376219) (Santa Cruz Biotechnology, Dallas, TX), IKKα: CST2682, NFKB2: CST4882, NIK: CST4994, p-RelA (p-p65) (CST3033), RelA (p65) (sc-8008), PPARγ: CST2443, RelB: CST4992, GAPDH: sc137179 and β-actin: sc69879.

RNA Isolation, cDNA Synthesis, and Quantitative-RT-PCR

Cells

Total RNA was isolated from cells by Purelink™ RNA Mini Kit (Life Technologies). cDNA was synthesized from 1 µg total RNA using iScript reverse transcription supermix (Bio-Rad, Hercules, CA) following the manufacturer's protocol. Quantitative RT-PCR was performed using iTaq Universal SYBR Green Supermix (Bio-Rad) with StepOnePlus Real-Time PCR System (Applied Biosystems, Foster City, CA).

Tissue

Mouse tissue was frozen with liquid nitrogen and ground to a powder with a pestle in a mortar (a minimum of 50mg of tissue is needed, for WAT 1g may be needed). Tissue was then lysed with Trizol (1mL per gram of tissue), followed by addition of chloroform to centrifuged supernatant (200µL chloroform: 1mL Trizol). Equal amounts of 70% ethanol was added to equal parts of

aqueous layer from sample in a new tube and then RNA was then collected in subsequent steps using Invitrogen Purelink RNA mini kit. Zymo DNAse was used with 40-80µL per sample. cDNA was synthesized from 2µg of RNA using iScript reverse transcriptase and buffer mix. Samples were ran in triplicate.

Target Gene	Forward Sequence	Reverse Sequence
SLC2a4 (GLUT4)	5'- GAA ACC CAT GCC GAC AAT GA -3'	5'- CTG TGC CAT CTT GAT GAC CG -3'
LEP (Leptin)	5'- TTC CTG GTG GCT TTG GTC CTA -3'	5'- AGC ACA TTT TGG GAA GGC AG -3'
AIPOQ (Adiponectin)	5'- GTT GCA AGC TCT CCT GTT CC -3'	5'- GAG CGA TAC ACA TAA GCG GC -3'
GPD1	5'- ACA CCC AAC TTT CGC ATC AC -3'	5'- TAG CAG GTC GTG ATG AGG TC -3'
GAPDH	5'- CTT TGT CAA GCT CAT TTC CTG G -3'	5'- TCT TGC TCA GTG TCC TTG C -3'
RPLP0	5'-AAG CGC GTC CTG GCA TTG TCT-3'	5'-CCG CAG GGG CAG CAG TGG T- 3'

3T3-L1 gene expression was normalized to GAPDH.

Mouse tissue gene expression was normalized to RPLP0.

Histology

Mouse tissue was fixed in 10% formalin for 24hrs. WAT was serially dehydrated in 50% ethanol for 2 days and then in 70% ethanol before processing and paraffin embedding. Liver stained with Oil Red O was fixed similarly, but then embedded in a tissue block with OCT for cryo-sectioning. WAT tissue was then stained with hematoxylin and eosin.

Whole Mount WAT Staining

Small portions of dissected gonadal adipose tissue were stained with BODIPY™ 490/509 (4,4-Difluoro-1,3,5,7,8-Pentamethyl-4-Bora-3a,4a-Diaza-s-Indacene) (Sigma Aldrich 790389) (5uM diluted 1:2500 in PBS) for 20 minutes at 37°C. Tissue was then then rinsed in PBS and fixed in 4% PFA overnight. Afterwards, the tissue is rinsed again and stained with Hoechst (1:1000) for 15 minutes. Tissues are then placed in an 8-chamber slide with PBS and imaged with a Nikon microscope.

Adipocyte Size Analysis

Adipocyte sizes were analyzed unbiasedly from 10x H&E histology or 10x whole mount BODIPY stained images in adiposoft plugin from ImageJ.

Animal Diet

Chow diet contained 4% fat while HFD diet contained 45% fat (Lab Supply 58125). Mice analyzed on a HFD were weaned from adults on a HFD and then maintained on a HFD for at least 2 months.

EchoMRI™

EchoMRI™ 100H machine was used to analyzed fat and lean mass of chow and HFD mice at 2 or 4 months of age. Mice were weighed before imaging and imaged in MRI tubes.

Metabolic Cages

Metabolic analysis on the mice was conducted in TSE Phenomaster™ metabolic cages through Rodent Preclinical Phenotyping Core at TAMU (https://genomics.tamu.edu/preclinical-

phenotyping/). Mice were weighed the day of and housed individually for 48hrs. Data was analyzed based on last 24hrs to compensate for mouse adjustment to the new environment.

Glucose Tolerance Testing

For glucose tolerance testing mice were morning fasted for 6hrs in clean cages. Mice were weighed and from tail clip initial glucose levels are recorded from glucose meter. The mice are then intraperitoneally injected with 20% D-glucose at 2g/kg (µL= 10 x BW). Blood glucose (in mg/dL) is then recorded at t=15, t=30, t=60, t=120 minutes post injection.

Insulin Tolerance Testing

For insulin tolerance testing mice were morning fasted for 4hrs in clean cages. Mice were weighed and from tail clip initial glucose levels are recorded using a glucose meter. The mice are then intraperitoneally injected with .5 U/kg Insulin (µL= 5 x BW of .1 U/mL insulin). Blood glucose (in mg/dL) is then recorded at t=15, t=30, t=45, t=60, t=90 minutes post injection.

Statistical Analysis

Statistical Analysis was done using GraphPad PRISM software, specifics on data representation and tests used for analysis can be found in figure legends. *p ≤.05, ** p ≤.01, *** p ≤.001, **** p≤.0001. Unpaired student t-tests were ran as two-tailed. All statistically significant analysis were ran based on a 95% confidence interval.

References

1. Pang, G., Xie, J., Chen, Q. & Hu, Z. Energy intake, metabolic homeostasis, and human health. *Food Science and Human Wellness* **3**, 89–103 (2014).
2. O'Brien, C. M., Mulukutla, B. C., Mashek, D. G. & Hu, W.-S. Regulation of Metabolic Homeostasis in Cell Culture Bioprocesses. *Trends in Biotechnology* **38**, 1113–1127 (2020).
3. Ma, Y. & Li, J. Metabolic Shifts during Aging and Pathology. *Compr Physiol* **5**, 667–686 (2015).
4. Li, T. *et al.* PKM2 coordinates glycolysis with mitochondrial fusion and oxidative phosphorylation. *Protein Cell* **10**, 583–594 (2019).
5. Yuan, X. *et al.* NAD + /NADH redox alterations reconfigure metabolism and rejuvenate senescent human mesenchymal stem cells in vitro. *Communications Biology* **3**, 1–15 (2020).
6. Duan, K. *et al.* Lactic acid induces lactate transport and glycolysis/OXPHOS interconversion in glioblastoma. *Biochem Biophys Res Commun* **503**, 888–894 (2018).
7. Bar-Even, A., Flamholz, A., Noor, E. & Milo, R. Rethinking glycolysis: on the biochemical logic of metabolic pathways. *Nature Chemical Biology* **8**, 509–517 (2012).
8. Rodic, S. & Vincent, M. D. Reactive oxygen species (ROS) are a key determinant of cancer's metabolic phenotype. *International Journal of Cancer* **142**, 440–448 (2018).
9. Li, X. *et al.* Mitochondria-Translocated PGK1 Functions as a Protein Kinase to Coordinate Glycolysis and the TCA Cycle in Tumorigenesis. *Mol Cell* **61**, 705–719 (2016).
10. Marchetti, P., Fovez, Q., Germain, N., Khamari, R. & Kluza, J. Mitochondrial spare respiratory capacity: Mechanisms, regulation, and significance in non-transformed and cancer cells. *The FASEB Journal* **34**, 13106–13124 (2020).
11. Sriskanthadevan, S. *et al.* AML cells have low spare reserve capacity in their respiratory chain that renders them susceptible to oxidative metabolic stress. *Blood* **125**, 2120–2130 (2015).

710 12. van der Windt, G. J. W. *et al.* Mitochondrial Respiratory Capacity Is a Critical Regulator of CD8+ T Cell
711 Memory Development. *Immunity* **36**, 68–78 (2012).
712 13. Huang, P. L. A comprehensive definition for metabolic syndrome. *Dis Model Mech* **2**, 231–237
713 (2009).
714 14. Prasun, P. Mitochondrial dysfunction in metabolic syndrome. *Biochimica et Biophysica Acta (BBA) -*
715 *Molecular Basis of Disease* **1866**, 165838 (2020).
716 15. Rosen, E. D. & Spiegelman, B. M. Adipocytes as regulators of energy balance and glucose
717 homeostasis. *Nature* **444**, 847–853 (2006).
718 16. Stern, J. H., Rutkowski, J. M. & Scherer, P. E. Adiponectin, Leptin, and Fatty Acids in the Maintenance
719 of Metabolic Homeostasis through Adipose Tissue Crosstalk. *Cell Metab* **23**, 770–84 (2016).
720 17. Choe, S. S., Huh, J. Y., Hwang, I. J., Kim, J. I. & Kim, J. B. Adipose Tissue Remodeling: Its Role in Energy
721 Metabolism and Metabolic Disorders. *Front Endocrinol (Lausanne)* **7**, 30 (2016).
722 18. Lee, B. C. & Lee, J. Cellular and molecular players in adipose tissue inflammation in the development
723 of obesity-induced insulin resistance. *Biochim Biophys Acta* **1842**, 446–62 (2014).
724 19. Yin, L. *et al.* Defective lymphotoxin-beta receptor-induced NF-kappaB transcriptional activity in NIK-
725 deficient mice. *Science* **291**, 2162–2165 (2001).
726 20. Akemi Matsushima, T. K. Essential role of nuclear factor (NF)-κB-inducing kinase and inhibitor of κB
727 (IκB) kinase α in NF-κB activation through lymphotoxin β receptor, but not through tumor necrosis
728 factor receptor I. *Journal of Experimental Medicine* **193**, 631–636 (2001).
729 21. Xiao, G., Fong, A. & Sun, S. C. Induction of p100 processing by NF-kappaB-inducing kinase involves
730 docking IkappaB kinase alpha (IKKalpha) to p100 and IKKalpha-mediated phosphorylation. *J Biol*
731 *Chem* **279**, 30099–105 (2004).
732 22. Sun, S. C. Non-canonical NF-kappaB signaling pathway. *Cell Res* **21**, 71–85 (2011).

733 23. Shinkura, R. *et al.* Alymphoplasia is caused by a point mutation in the mouse gene encoding Nf-κb-
734 inducing kinase. *Nature Genetics* **22**, 74–77 (1999).
735 24. Brightbill, H. D. *et al.* Conditional Deletion of NF-kappaB-Inducing Kinase (NIK) in Adult Mice Disrupts
736 Mature B Cell Survival and Activation. *J Immunol* **195**, 953–64 (2015).
737 25. Li, Y. *et al.* Cell intrinsic role of NF-kappaB-inducing kinase in regulating T cell-mediated immune and
738 autoimmune responses. *Sci Rep* **6**, 22115 (2016).
739 26. Lacher, S. M. *et al.* NF-κB inducing kinase (NIK) is an essential post-transcriptional regulator of T-cell
740 activation affecting F-actin dynamics and TCR signaling. *Journal of Autoimmunity* **94**, 110–121
741 (2018).
742 27. Hamdan, T. A. *et al.* Map3k14 as a Regulator of Innate and Adaptive Immune Response during Acute
743 Viral Infection. *Pathogens* **9**, (2020).
744 28. Gu, M. *et al.* NF-κB-inducing kinase maintains T cell metabolic fitness in antitumor immunity. *Nat*
745 *Immunol* **22**, 193–204 (2021).
746 29. Jung, J. U. *et al.* NIK/MAP3K14 Regulates Mitochondrial Dynamics and Trafficking to Promote Cell
747 Invasion. *Curr Biol* **26**, 3288–3302 (2016).
748 30. Kamradt, M. L. *et al.* NIK promotes metabolic adaptation of glioblastoma cells to bioenergetic stress.
749 *Cell Death & Disease* **12**, 1–18 (2021).
750 31. Sheng, L. *et al.* NF-kappaB-inducing kinase (NIK) promotes hyperglycemia and glucose intolerance in
751 obesity by augmenting glucagon action. *Nat Med* **18**, 943–9 (2012).
752 32. Liu, Y. *et al.* Liver NF-κB-Inducing Kinase Promotes Liver Steatosis and Glucose Counterregulation in
753 Male Mice With Obesity. *Endocrinology* **158**, 1207–1216 (2017).
754 33. Li, Y. *et al.* NIK links inflammation to hepatic steatosis by suppressing PPARα in alcoholic liver
755 disease. *Theranostics* **10**, 3579–3593 (2020).

756 34. Mota, M., Banini, B. A., Cazanave, S. C. & Sanyal, A. J. Molecular mechanisms of lipotoxicity and
757 glucotoxicity in nonalcoholic fatty liver disease. *Metabolism* **65**, 1049–61 (2016).
758 35. Pan, X. *et al.* Adipogenic changes of hepatocytes in a high-fat diet-induced fatty liver mice model
759 and non-alcoholic fatty liver disease patients. *Endocrine* **48**, 834–47 (2015).
760 36. Even, P. C. & Nadkarni, N. A. Indirect calorimetry in laboratory mice and rats: principles, practical
761 considerations, interpretation and perspectives. *American Journal of Physiology-Regulatory,*
762 *Integrative and Comparative Physiology* **303**, R459–R476 (2012).
763 37. Li, Z. *et al.* Discovery of a Potent and Selective NF-κB-Inducing Kinase (NIK) Inhibitor That Has Anti-
764 inflammatory Effects in Vitro and in Vivo. *J. Med. Chem.* **63**, 4388–4407 (2020).
765 38. Rosen, E. D. C/EBPalpha induces adipogenesis through PPARgamma : a unified pathway. *Genes &*
766 *Development* **16**, 22–26 (2002).
767 39. Calabrese, C. *et al.* Respiratory complex I is essential to induce a Warburg profile in mitochondria-
768 defective tumor cells. *Cancer & Metabolism* **1**, 11 (2013).
769 40. Liberti, M. V. & Locasale, J. W. The Warburg Effect: How Does it Benefit Cancer Cells? *Trends*
770 *Biochem Sci* **41**, 211–218 (2016).
771 41. Mauvais-Jarvis, F. Sex differences in metabolic homeostasis, diabetes, and obesity. *Biol Sex Differ* **6**,
772 (2015).
773 42. Riant, E. *et al.* Estrogens Protect against High-Fat Diet-Induced Insulin Resistance and Glucose
774 Intolerance in Mice. *Endocrinology* **150**, 2109–2117 (2009).
775 43. Handgraaf, S. *et al.* Prevention of Obesity and Insulin Resistance by Estrogens Requires ER Activation
776 Function-2 (ER AF-2), Whereas ER AF-1 Is Dispensable. *Diabetes* **62**, 4098–4108 (2013).
777 44. Klein, S. L. & Flanagan, K. L. Sex differences in immune responses. *Nature Reviews Immunology* **16**,
778 626–638 (2016).

779 45. Eisenreich, W., Rudel, T., Heesemann, J. & Goebel, W. How Viral and Intracellular Bacterial
780 Pathogens Reprogram the Metabolism of Host Cells to Allow Their Intracellular Replication. *Front.*
781 *Cell. Infect. Microbiol.* **9**, (2019).
782 46. Sanchez, E. L. & Lagunoff, M. Viral activation of cellular metabolism. *Virology* **479–480**, 609–618
783 (2015).
784 47. Tang, T. *et al.* Uncoupling of inflammation and insulin resistance by NF-kappaB in transgenic mice
785 through elevated energy expenditure. *J Biol Chem* **285**, 4637–44 (2010).
786 48. Pascal Peraldi, M. X. Thiazolidinediones Block Tumor Necrosis Factor-a-induced Inhibition of insulin
787 signaling. *J. Clin. Invest.* **Volume 100**, 1863–1869 (1997).
788 49. Berg, A. H., Lin, Y., Lisanti, M. P. & Scherer, P. E. Adipocyte differentiation induces dynamic changes
789 in NF-κB expression and activity. *American Journal of Physiology-Endocrinology and Metabolism*
790 **287**, E1178–E1188 (2004).
791 50. Weidemann, A. *et al.* Classical and alternative NF-kappaB signaling cooperate in regulating
792 adipocyte differentiation and function. *Int J Obes (Lond)* **40**, 452–9 (2016).
793 51. Zhao, P. *et al.* TBK1 at the Crossroads of Inflammation and Energy Homeostasis in Adipose Tissue.
794 *Cell* **172**, 731-743.e12 (2018).
795 52. Bugge, A., Dib, L. & Collins, S. Measuring respiratory activity of adipocytes and adipose tissues in real
796 time. *Methods Enzymol* **538**, 233–247 (2014).
797

NF-κB-Inducing Kinase Rewires Metabolic Homeostasis and Promotes Diet-Induced Obesity

Authors: Kathryn M. Pflug, Dong W. Lee, Raquel Sitcheran

Supplemental Data

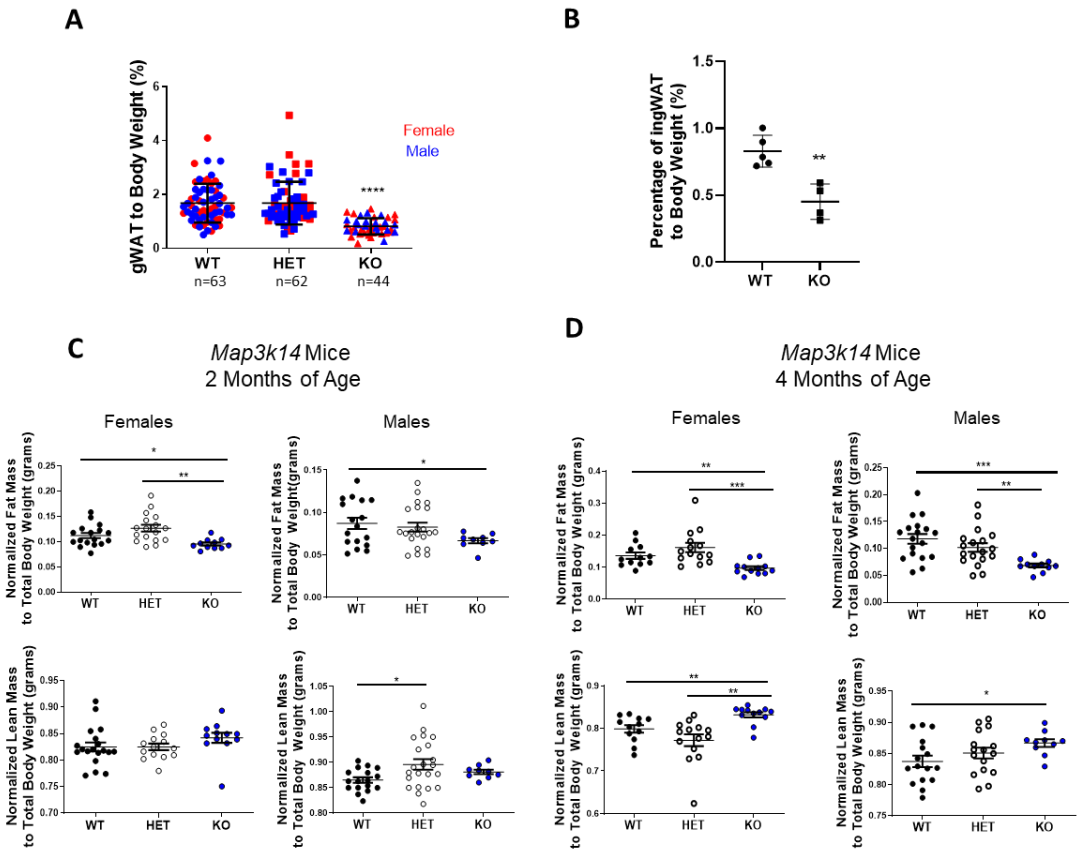

Supplemental Figure 1.

(A) Weights of 4-month-old chow fed WT, HET, and NIK KO male and female gonadal WAT on a chow diet. Data are represented as mean ± SD, **** p ≤.0001, Tukey Multiple Comparison Test. **(B)** Analysis of inguinal WAT from chow fed male WT and NIK KO mice. Data represented as mean ± SD, ** p ≤.01, Unpaired Student t-test. **(C)** Echo MRI data of fat and lean mass ratios of male and female MAP3K14 mice at 2 months and **(D)** 4 months of age. Data mean ± SEM, * p≤.05, ** p ≤.01, *** p ≤.001, Unpaired Student t-test.

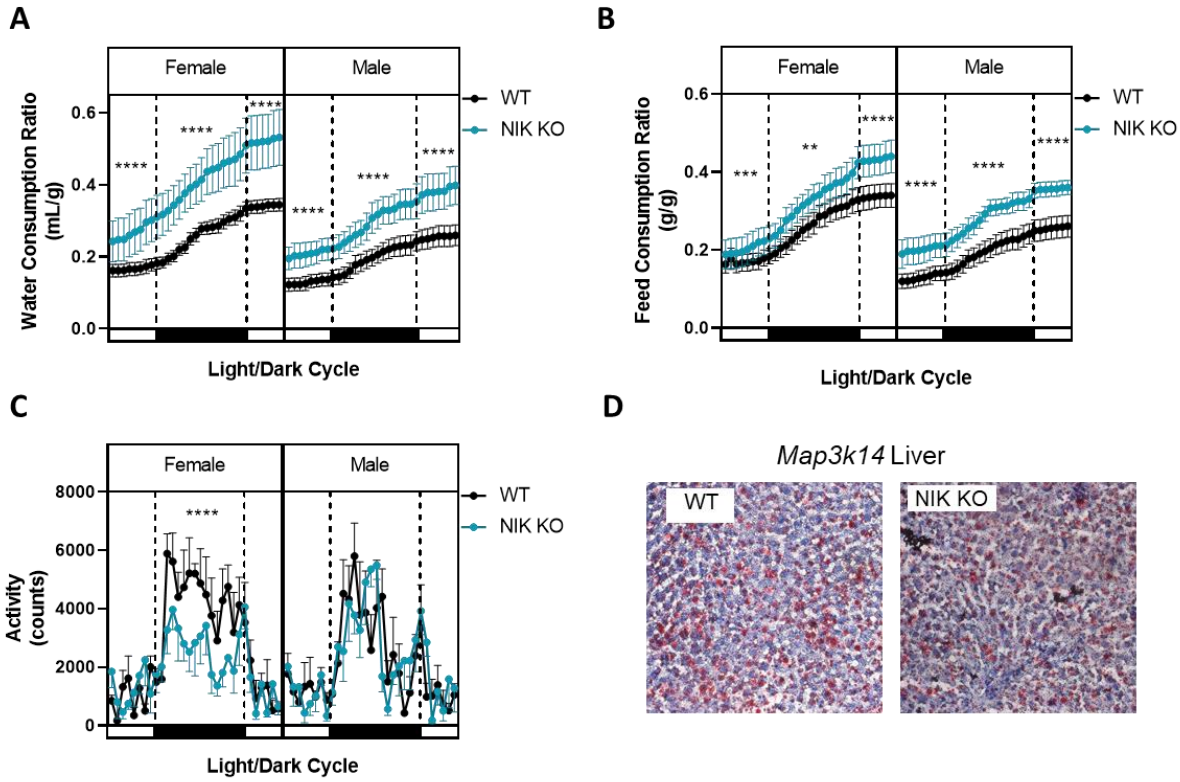

Supplemental Figure 2.

Metabolic cage data of male and female WT, HET, NIK KO mice at 4 months of age for **(A)** water consumption, **(B)** food consumption and **(C)** activity. Data are represented as mean ± SEM, *p≤.05, ** p ≤.01, **** p ≤.0001, Unpaired Student t-test. **(D)** Oil Red O and hematoxylin staining of liver sections from chow fed WT and NIK KO mice.

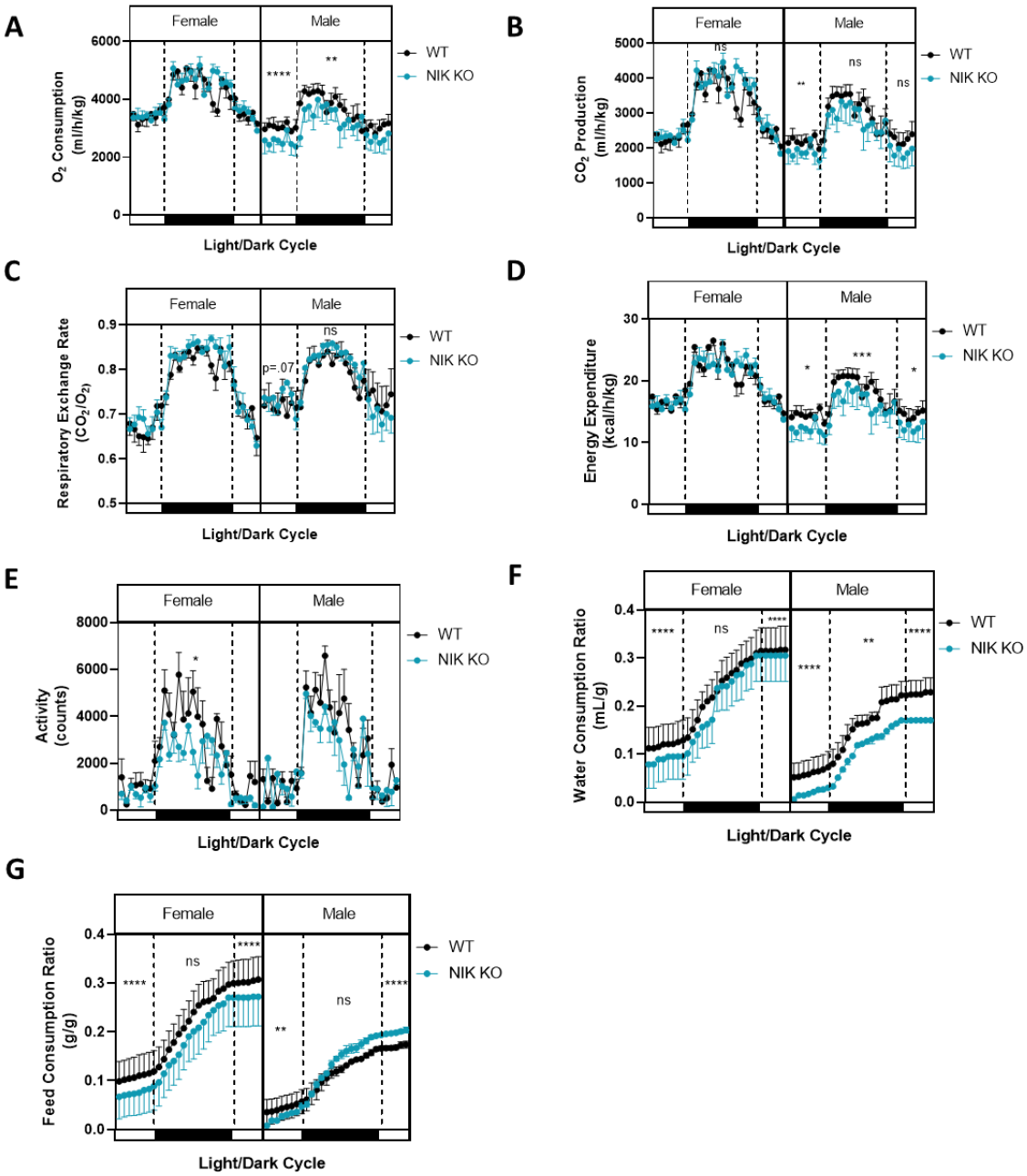

Supplemental Figure 3.

(A-G) Analysis of a 24hr period of metabolic cage data. Representing chow fed male and female, WT and NIK KO mice at 2 months of age. Data are represented as mean ± SEM, *p≤.05, ** p ≤.01,***p ≤.001, **** p ≤.0001, Unpaired Student t-test.

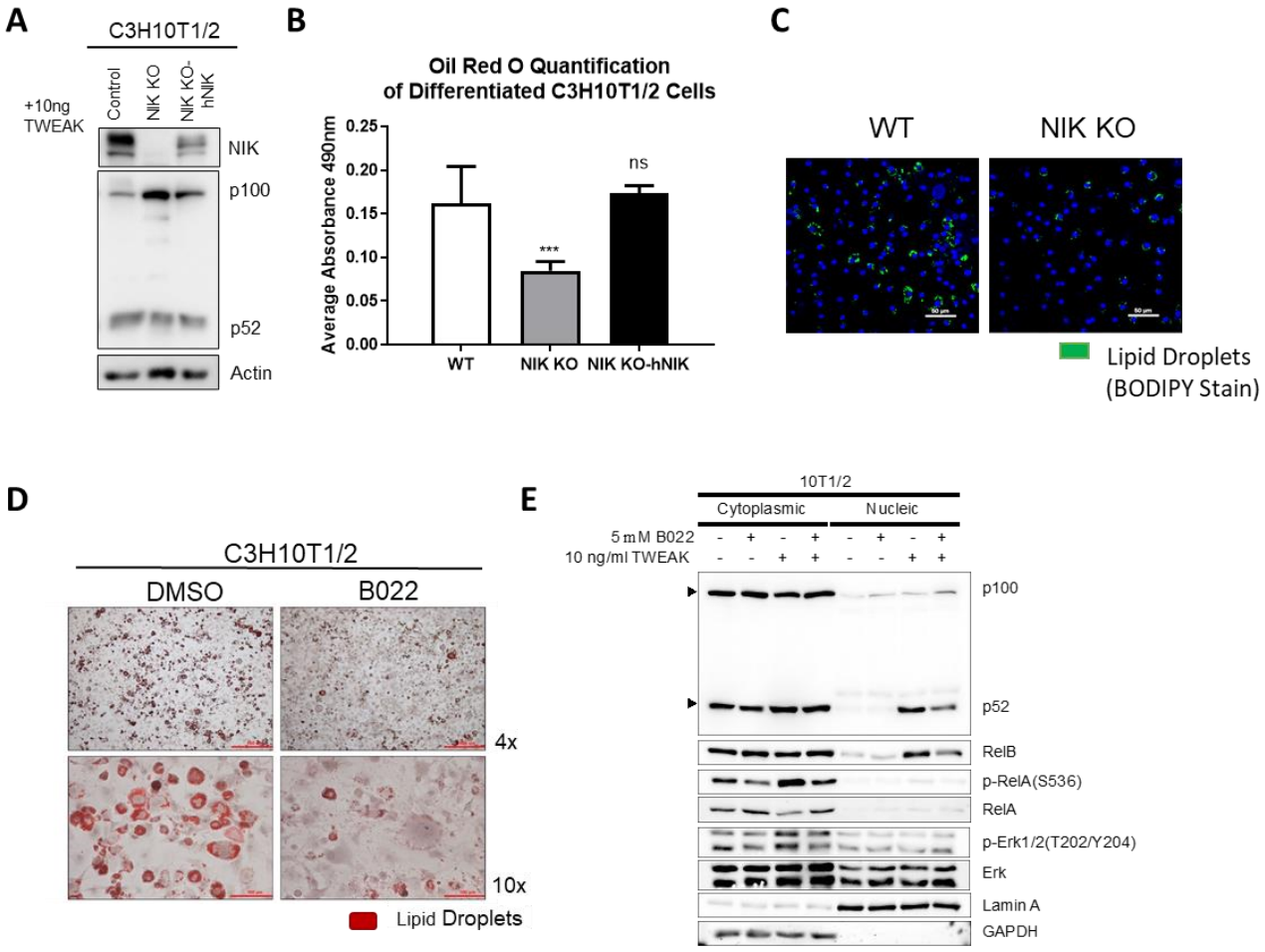

Supplemental Figure 4.

(A) Blot of C3H10T1/2 cells confirming the loss of NIK (NIK KO) and the rescue of non-canonical NF-κB functionality (p100-p52 processing) with the reestablishment of human NIK (NIK KO-hNIK). **(B)** Quantification of oil red o staining of differentiated C3H10T1/2 cells. Data represented as mean ± SD, * p≤.05, ** p ≤.01, *** p ≤.001, **** p ≤.0001, Tukey's Multiple Comparison Test. **(C)** Adipocyte differentiation of primary bone marrow cells from WT and NIK KO mice stained with BODIPY (lipid droplets; green) and Hoechst (blue). **(D)** C3H10T1/2 cells treated with DMSO or the NIK inhibitor (B022), induced for adipocyte differentiation, and then stained with oil red o. **(E)** Cytoplasmic/ nuclear fractionation of C3H10T1/2 cells treated with B022 (NIK inhibitor) or TWEAK (activator of the noncanonical NF-κB pathway), showing inhibition of p100-p52 processing (induction of noncanonical protein processing by NIK) with B022 treatment.

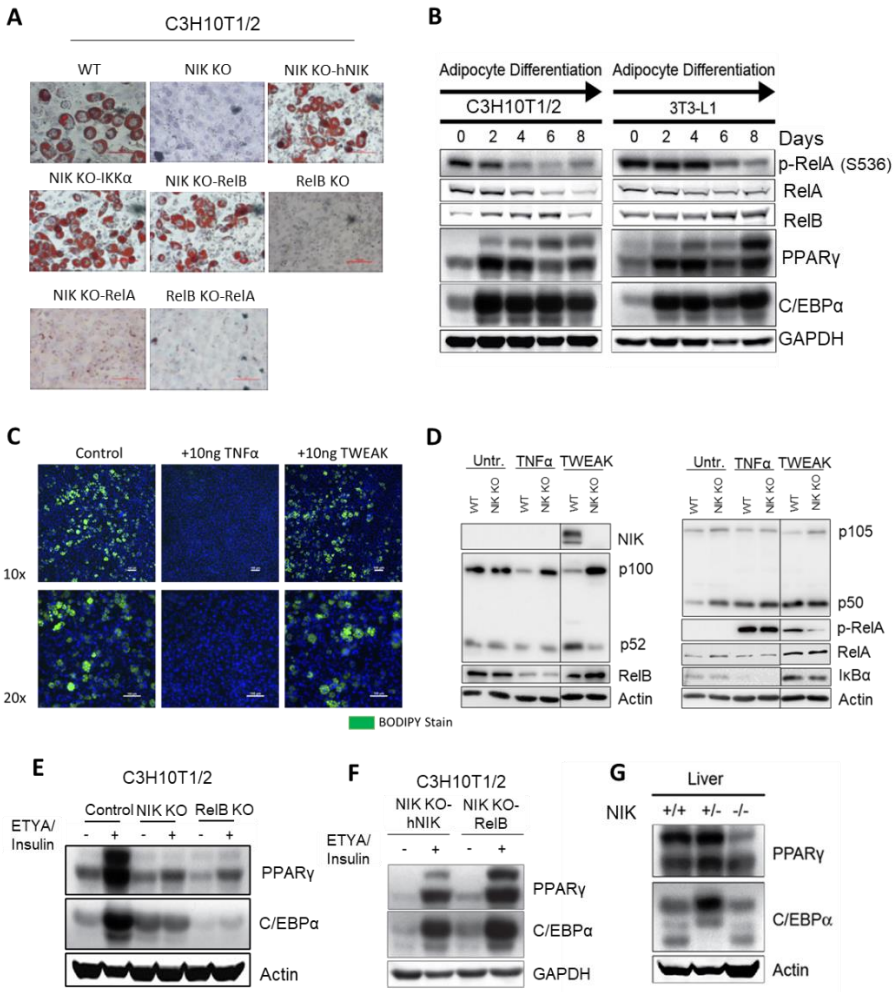

Supplemental Figure 5.

(A) Oil Red O staining of C3H10T1/2 cells after induction of adipocyte differentiation with ETYA and insulin. **(B)** Immunoblot of adipocyte induction in C3H10T1/2 and 3T3-L1 cells with ETYA/Insulin. **(C)** BODIPY staining of lipid droplets (green) and Hoechst staining (blue) in differentiated C3H10T1/2 treated with TNFα (tumor necrosis factor alpha; activator of canonical NF-κB pathway) or TWEAK (tumor necrosis weak life factor; activator of noncanonical NF-κB pathway). **(D)** Immunoblots confirming activation of the noncanonical or canonical NF-κB pathway after induction with TWEAK or TNFα, respectively. Immunoblot of transcriptional activators of adipogenesis, PPARγ and C/EBPα expression in undifferentiated and differentiated **(E)** NIK KO, RelB KO, **(F)** NIK KO-hNIK and NIK KO-RelB C3H10T1/2 cells, **(G)** and mouse liver samples.

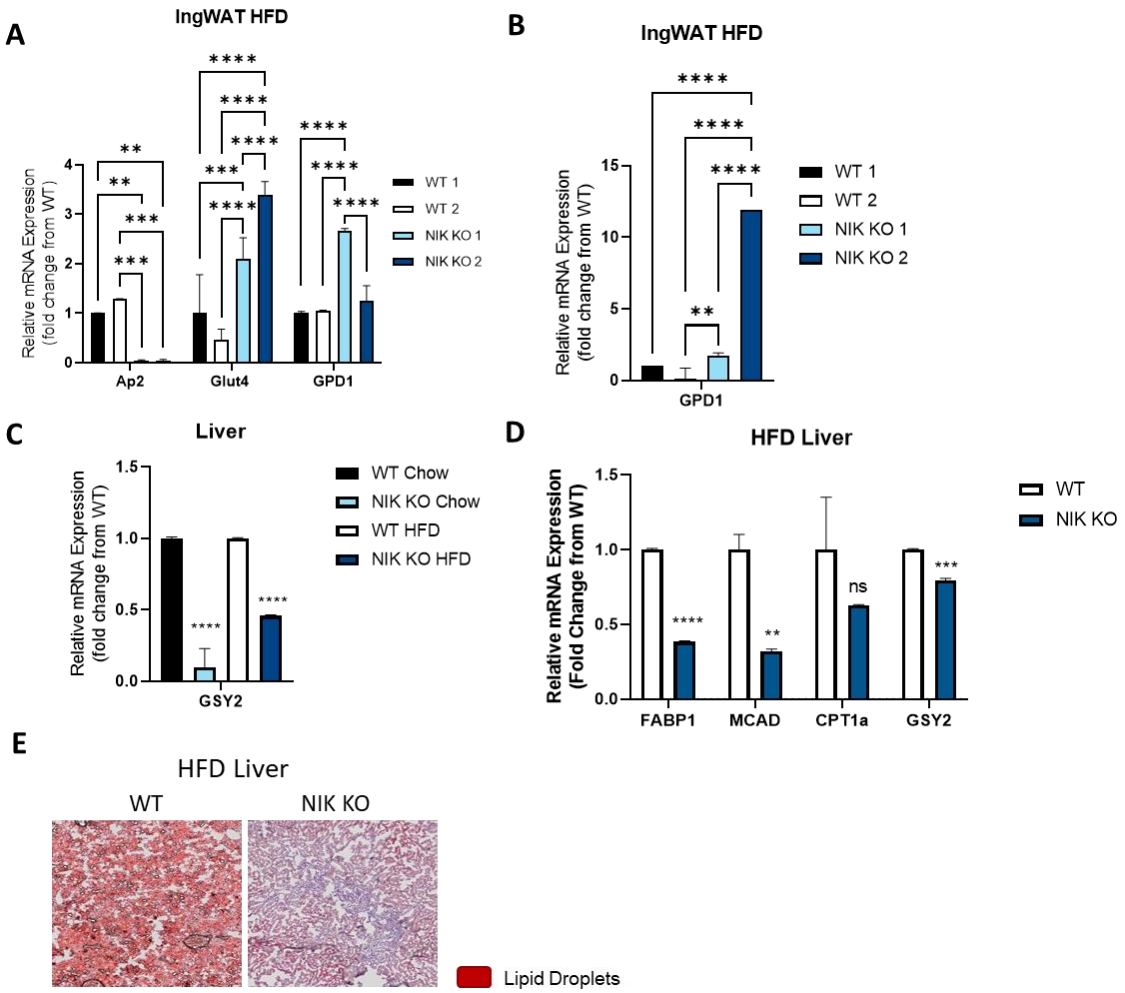

Supplemental Figure 6.

(A) qPCR analysis of adipocyte genes Ap2 (adipocyte specific protein 2; FABP4), GLUT4 (glucose transporter 4, SLC2A4), GPD1 (glucose-3-phosphate dehydrogenase 1) of inguinal WAT from male HFD mice. **(B)** GPD1 mRNA analysis of inguinal WAT from HFD female mice. **(C)** GSY2 (glycogen synthase 2) relative mRNA expression from chow and HFD liver samples. **(D)** qPCR analysis of fatty acid oxidation genes (FAB1; fatty acid binding protein, MCAD; medium chain acyl-CoA dehydrogenase, CPT1α; carnitine protein transferase) and glycogen synthase 2 from HFD female liver samples. N=2 biological replicates ran in triplicate **(A-D)** Data represented as mean ± SD, Unpaired Student t-test. **(E)** Oil Red O and hematoxylin staining for lipid accumulation in liver samples of HFD mice.